Four-lepton LHC events from MSSM Higgs boson decays into neutralino and chargino pairs

TUHEP-TH-07161
SCUPHY-07002
SHEP-07-12
DFTT 40/2009

Mike Bisset*, Jun Li
Center for High Energy Physics and Department of Physics, Tsinghua University, Beijing, 100084 P.R. China

Nick Kersting*
Physics Department, Sichuan University, Chengdu, 610065 P.R. China

Ran Lu*
Physics Department, University of Michigan, Ann Arbor, MI 48109, USA

Filip Moortgat*
Department of Physics, CERN, CH-1211, Geneva 23, Switzerland

Stefano Moretti*
School of Physics and Astronomy, University of Southampton, Highfield, Southampton SO17 1BJ, UK

and

Dipartimento di Fisica Teorica, Università degli Studi di Torino Via Pietro Giuria 1, 10125 Torino, Italy

Abstract

Heavy neutral Higgs boson production and decay into neutralino and chargino pairs is studied at the Large Hadron Collider in the context of the minimal supersymmetric standard model. Higgs boson decays into the heavier neutralino and chargino states, *i.e.*, $H^0, A^0 \to \widetilde{\chi}_2^0\widetilde{\chi}_3^0, \widetilde{\chi}_2^0\widetilde{\chi}_4^0, \widetilde{\chi}_3^0\widetilde{\chi}_3^0, \widetilde{\chi}_3^0\widetilde{\chi}_4^0, \widetilde{\chi}_4^0\widetilde{\chi}_4^0$ as well as $H^0, A^0 \to \widetilde{\chi}_1^\pm\widetilde{\chi}_2^\mp, \widetilde{\chi}_2^+\widetilde{\chi}_2^-$ (all leading to four-lepton plus missing transverse energy final states), is found to improve the possibilities of discovering such Higgs states beyond those previously identified by considering $H^0, A^0 \to \widetilde{\chi}_2^0\widetilde{\chi}_2^0$ decays only. In particular, H^0, A^0 bosons with quite heavy masses, approaching $\sim$800 GeV in the so-called 'decoupling region' where no clear SM signatures for the heavier MSSM Higgs bosons are known to exist, can now be discerned, for suitable but not particularly restrictive configurations of the low energy supersymmetric parameters. The high M_A discovery reach for the H^0 and A^0 may thus be greatly extended. Full event-generator level simulations, including realistic detector effects and analyses of all significant backgrounds, are performed to delineate the potential H^0, A^0 discovery regions. The wedgebox plot technique is also utilized to further analyze the 4ℓ plus missing transverse energy signal and background events. This study marks the first thorough and reasonably complete analysis of this important class of MSSM Higgs boson signature modes. In fact, this is the first time discovery regions including all possible neutralino and chargino decay modes of the Higgs bosons have ever been mapped out.

1 Introduction

Among the most investigated extensions of the standard model (SM) are those incorporating supersymmetry (SUSY), and among these the one with the fewest allowable number of new particles and interactions, the minimal supersymmetric standard model (MSSM), has certainly received considerable attention. Yet, when prospective signals at the Large Hadron Collider (LHC) of the new particle states within the MSSM are considered, there is still much that needs clarification. Nothing underscores this more than the MSSM electroweak symmetry breaking (EWSB) Higgs sector. Included therein is a quintet of Higgs bosons left from the two $SU(2)_L$ Higgs doublets after EWSB (see [1, 2] for more details): a charged pair, $H^\pm$, the neutral CP-odd A^0 and the neutral CP-even h^0 and H^0 (with $M_h < M_H$). The entire Higgs sector (*i.e.*, masses and couplings to ordinary matter) can be described at tree-level by only two independent parameters: the mass of one of the five Higgs states (*e.g.*, M_A) and the ratio of the vacuum expectation values of the two Higgs doublets (denoted by $\tan\beta$). These must be augmented to include significant radiative corrections which most notably raise the upper limit on the mass of the light Higgs boson from $M_h \leq M_Z$ at tree-level to $\lesssim 140\,\text{GeV}$ ($150\,\text{GeV}$) with inclusion of corrections up to two loops and assuming a stop-sector scale of $M_{SUSY} = 1\,\text{TeV}$ ($2\,\text{TeV}$) and $m_t = (178.0 \pm 4.3)\,\text{GeV}$ according to [3], or $\lesssim 135\,\text{GeV}$ with $m_t = (172.6 \pm 1.4)\,\text{GeV}$ by [4] (stop mass range not specified). This definite upper bound will allow experimentalists to definitively rule out such a minimal SUSY scenario at the LHC if such a light Higgs state is not observed. Thus, the possible production and decay modes of the h^0 state have understandably been investigated in quite some detail [2]. In contrast, the possibilities for the other heavier neutral MSSM Higgs bosons have not been so thoroughly examined. Yet it is crucial that the avenues for discovery of these other MSSM Higgs bosons be well understood since, even if a candidate for h^0 discovery is experimentally identified, it may be indistinguishable from a SM Higgs boson (this corresponds to the so-called 'decoupling region', with $M_H, M_A \gg 200\,\text{GeV}$ and for intermediate to large values of $\tan\beta$ [2, 5]). Then the additional identification of heavier Higgs bosons may well be required to establish that there is in fact an extended Higgs sector beyond the single doublet predicted by the SM.

Finding signatures for these heavier MSSM Higgs bosons has proved to be challenging. Unlike the lone Higgs boson of the SM of similar mass, couplings of these MSSM Higgs bosons to SM gauge bosons are either absent at tree level (for A^0) or strongly suppressed over much of the allowed parameter space (for H^0). Thus, identification of A^0 and H^0 via their decays into known SM particles relies chiefly on decays of said Higgs bosons into the heaviest fermions available, namely, tau leptons and bottom quarks[1]. Identification of hadronic decays/jet showers of these third generation fermions may be problematic in the QCD-rich environment of the LHC[2], so that it is very questionable that the entire parameter space can be covered with just SM-like signatures. Fortunately, in the MSSM there is an alternative: decays of these Higgs bosons into sparticles, in particular the charginos and neutralinos[3] formed from the EW gauginos and Higgsinos. Higgs boson couplings to certain –ino states may be substantial, and these heavy sparticles may themselves decay — except for $\widetilde{\chi}_1^0$ which is assumed to be the stable

[1] H^0, A^0 top quark couplings are suppressed relative to a SM Higgs boson of the same mass.

[2] In addition, jet-free events from Higgs boson decays to tau-lepton pairs where both tau-leptons in turn decay leptonically also come with considerable background-separation challenges [6].

[3] In the remainder, charginos and neutralinos collectively will be abbreviated by '–inos'.

lightest supersymmetric particle (LSP) — in readily-identifiable ways (such as into leptons) to provide a clean experimental signature.

A number of previous articles [7, 8, 9, 10, 11] as well as at least one Ph.D. thesis [12] have focused on the signal potential of the decays of the heavier neutral MSSM Higgs bosons into neutralinos and charginos:

$$H^0, A^0 \to \widetilde{\chi}_a^+ \widetilde{\chi}_b^-, \widetilde{\chi}_i^0 \widetilde{\chi}_j^0 \qquad (a, b = 1, 2, \;\; i, j = 1, 2, 3, 4). \tag{1}$$

Therein only subsequent –ino decays into leptons (which will be taken to mean electrons and/or muons, $\ell = e, \mu$) were considered, as this is preferable from the standpoint of LHC detection. Since relatively light sleptons can greatly enhance [13, 20, 21] the branching ratios (BRs) for such decays, the properties of the slepton sector of the MSSM also need to be specified. All of the previous works concentrated almost[4] exclusively on the decays $H^0, A^0 \to \widetilde{\chi}_2^0 \widetilde{\chi}_2^0$. In addition, the subsequent neutralino decays $\widetilde{\chi}_2^0 \to \widetilde{\chi}_1^0 \ell^+ \ell^-$ were typically presumed to proceed via three-body decays with an off-mass-shell intermediate Z^{0*} or slepton, neglecting the possibility of the intermediate Z^0 or slepton being on-mass-shell ([22] and [23] delve in considerable depth into the distinctions between these cases).

In this work[5], *all* the decays in (1) are incorporated. In fact, as the presumed mass of a Higgs boson grows, more such decay modes will become accessible. Therefore, if decay channels to the heavier -inos are significant, they may provide signatures for heavier neutral Higgs bosons (with masses well into the aforementioned decoupling region). When heavier –ino states are included, it also becomes easier to construct model spectra with slepton masses lying below those of the heavier –inos. Thus, in this work, intermediate sleptons are allowed to be both on- and off-mass-shell (same for the $Z^{0(*)}$)[6]. More background channels are also emulated than in previous studies. The Higgs boson production modes considered herein are $gg \to H^0, A^0$ (gluon-fusion) and $q\bar{q} \to H^0, A^0$ (quark-fusion). (The second mode is dominated by the case $q = b$.)

This work is organized as follows. The next section provides an overview of the MSSM parameter space through calculation of inclusive rates for the relevant production and decay processes contributing to the signal. Sect. 3 then specializes these results to the more restrictive minimal supergravity (mSUGRA) scenario for SUSY breaking. Sect. 4 gives the numerical results for the signal and background processes based upon Monte Carlo (MC) simulations of parton shower (PS) and hadronization as well as detector effects. This includes mapping out discovery regions for the LHC. The recently-introduced 'wedgebox' method of [27], which is reminiscent of the time-honored Dalitz plot technique, is utilized in Sect. 5 to extract information about the –ino mass spectra and the –ino couplings to the Higgs bosons. Finally, the last section presents conclusions which can be drawn from this study.

[4]The decays $H^0, A^0 \to \widetilde{\chi}_1^+ \widetilde{\chi}_1^-, \widetilde{\chi}_1^0 \widetilde{\chi}_2^0$ were also studied in [7] but found to be unproductive due to large backgrounds to the resulting di-lepton signals.

[5]A preliminary account of this analysis is given in Ref. [24].

[6]Similar studies for charged Higgs boson decays into a neutralino and a chargino, where the charged Higgs boson is produced in association with a t or $\bar{t}$ quark are done in [13, 20] (see also Refs. [25, 26]).

2 MSSM parameter space

As noted above, M_A and $\tan\beta$ may be chosen as the MSSM inputs characterizing the MSSM Higgs bosons' decays into SM particles[7]. But when Higgs boson decays to –inos are included, new MSSM inputs specifying the –ino sector also become crucial. To identify the latter, the already mentioned Higgs/Higgsino mixing mass, μ, and the SUSY-breaking $SU(2)_L$ gaugino mass, M_2, in addition to $\tan\beta$, are required. The SUSY-breaking $U(1)_Y$ gaugino mass, M_1, is assumed to be determined from M_2 via gaugino unification (*i.e.*, $M_1 = \frac{5}{3}\tan^2\theta_W M_2$). This will fix the tree-level –ino masses (to which the radiative corrections are quite modest) along with their couplings to the Higgs bosons.

Inputs (assumed to be flavor-diagonal) from the slepton sector are the left and right soft slepton masses for each of the three generations (selectrons, smuons, and staus) and the trilinear 'A-terms' which come attached to Yukawa factors and thus only A_τ has a potential impact. *A priori*, all six left and right mass inputs (and A_τ) are independent. However, in most models currently advocated, one has $m_{\widetilde{e}_R} \simeq m_{\widetilde{\mu}_R}$ and $m_{\widetilde{e}_L} \simeq m_{\widetilde{\mu}_L}$. Herein these equalities are assumed to hold.

2.1 Experimental limits

To maximize leptonic –ino BR enhancement, sleptons should be made as light as possible. But direct searches at LEP [28, 29] place significant limits on slepton masses: $m_{\widetilde{e}_1} \geq 99.0\,\text{GeV}$, $m_{\widetilde{\mu}_1} \geq 91.0\,\text{GeV}$, $m_{\widetilde{\tau}_1} \geq 85.0\,\text{GeV}$ (these assume that the slepton is not nearly-degenerate with the LSP) and $m_{\widetilde{\nu}} \geq 43.7\,\text{GeV}$ (from studies at the Z^0 pole). Furthermore, the sneutrino masses are closely tied to the left soft mass inputs, and, to avoid extra controversial assumptions, only regions of the MSSM parameter space where the LSP is the lightest neutralino rather than a sneutrino will be considered[8]. To optimize the –ino leptonic BRs without running afoul of the LEP limits, it is best[9] to set $m_{\widetilde{\ell}_R} = m_{\widetilde{\ell}_L}$. If all three generations have the same soft inputs (with $A_\tau = A_\ell = 0$), then the slepton sector is effectively reduced to one optimal input value (defined as $m_{\widetilde{\ell}_{soft}} \equiv m_{\widetilde{\ell}_{L,R}}$). However, since –ino decays into tau-leptons are generally not anywhere near as beneficial as those into electrons or muons, it would be even better if the stau inputs were significantly above those of the first two generations. This would enhance the –inos' BRs into electrons and muons. In the general MSSM, one is of course free to choose the inputs as such. Doing so would also weaken restrictions from LEP, especially for high values of $\tan\beta$. Fig. 1 in [20] shows values for this optimal slepton mass over the M_2–μ plane

[7]Several other MSSM inputs also enter into the radiatively-corrected MSSM Higgs boson masses and couplings of the MSSM Higgs bosons to SM particles, namely, inputs from the stop sector — the soft SUSY-breaking stop trilinear coupling A_t plus the stop masses — and the Higgs/Higgsino mixing mass μ. In the present work the stop masses are assumed to be heavy ($\approx 1\,\text{TeV}$) whereas A_t is fixed to zero. The μ parameter is not crucial for the SM decay modes; however, it will become so when decays to –inos are considered.

[8]Further, if a sneutrino were the LSP and thus presumably the main constituent of galactic dark matter, its strong couplings to SM EW gauge bosons would lead to event rates probably inconsistent with those observed by Super-Kamiokande. In contrast, the coupling of an –ino to SM EW gauge bosons can be tuned to obtain rates consistent with current experimental limits.

[9]Unless this leads to $m_{\widetilde{\nu}} < m_{\widetilde{\chi}_2^0} < m_{\widetilde{\ell}^\pm}$, in which case $\widetilde{\chi}_2^0$ decays to charged leptons will be suppressed with respect to $\widetilde{\chi}_2^0$ decays to neutrinos, to avoid which having $m_{\widetilde{\ell}_R} < m_{\widetilde{\ell}_L}$ is preferred.

relevant to the –ino sector for $\tan\beta = 10, 20$. Setting the soft stau mass inputs 100 GeV above those of the other soft slepton masses, as will often be done herein, complies with current experimental constraints and moderately enhances the signal rates [24].

2.2 The signal inclusive cross sections

Figs. 1, 2 and 3 show the LHC rates (in fb) for $\sigma(pp \to H^0) \times \mathrm{BR}(H^0 \to 4\ell N) + \sigma(pp \to A^0) \times \mathrm{BR}(A^0 \to 4\ell N)$, where N is any number (including zero) of invisible neutral particles (in the MSSM these are either neutrinos or $\widetilde{\chi}_1^0$ LSPs) obtained for $\tan\beta = 5$, 10, and 20, respectively[10]. (Hereafter this sum of processes will be abbreviated by $\sigma(pp \to H^0, A^0) \times \mathrm{BR}(H^0, A^0 \to 4\ell N)$.) Each figure gives separate scans of the μ *vs.* M_2 plane most relevant to the –ino sector for (from top to bottom) $M_A = 400$, 500, and 600 GeV — covering the range of Higgs boson masses of greatest interest [24]. This is in the region of the MSSM parameter space where observation of h^0 alone may be insufficient to distinguish the MSSM Higgs sector from the SM case (*i.e.*, the decoupling region). The darkened zones seen around the lower, inner corner of each plot are the regions excluded by the experimental results from LEP.

First observe that these 'raw' or 'inclusive' (*i.e.*, before applying selection cuts to the basic event-type) rates may be sufficiently large. For an integrated luminosity of 100 fb^{-1}, the peak raw event number is around 4000(1700) events for $M_A = 400(600)$ GeV and $\tan\beta = 20$, irrespective of the sign of μ. Also observe that low values of $|\mu|$ and M_2 yield the highest signal rates, though significant event numbers are also found when one but not the other of these parameters is increased (especially $|\mu|$; rates do fall rapidly when M_2 increases much beyond 500 GeV). These numbers are substantial (especially at high $\tan\beta$) and, if experimental efficiencies are good, they may facilitate a much more accurate determination of some masses or at least mass differences in the -ino spectrum as well as the Higgs-ino mass differences than those achieved in previous studies based solely on $H^0, A^0 \to \widetilde{\chi}_2^0\widetilde{\chi}_2^0$ decays.

Note the color coding of the three figures depicting what percentage of the signal events are coming from Higgs boson decays to $\widetilde{\chi}_2^0\widetilde{\chi}_2^0$: $> 90\%$ in the red zones, from 90% down to 50% in the yellow zones, from 50% to 10% in the blue zones, and $< 10\%$ in uncolored regions. If the events are not coming from $\widetilde{\chi}_2^0\widetilde{\chi}_2^0$, then they are almost always from Higgs boson decays including heavier neutralinos, *i.e.*, $H^0, A^0 \to \widetilde{\chi}_2^0\widetilde{\chi}_3^0, \widetilde{\chi}_2^0\widetilde{\chi}_4^0, \widetilde{\chi}_3^0\widetilde{\chi}_3^0, \widetilde{\chi}_3^0\widetilde{\chi}_4^0, \widetilde{\chi}_4^0\widetilde{\chi}_4^0$ (possibly also with contributions from $H^0, A^0 \to \widetilde{\chi}_1^\pm\widetilde{\chi}_2^\mp, \widetilde{\chi}_2^+\widetilde{\chi}_2^-$ which are also taken into account here). Also note that the main source of events at the optimal location in the –ino parameter space shifts from $\widetilde{\chi}_2^0\widetilde{\chi}_2^0$ to heavier –ino pairs as M_A grows from 400 to 600 GeV. Irrespective of the heavier Higgs boson masses, Higgs boson decays to $\widetilde{\chi}_2^0\widetilde{\chi}_2^0$ are the dominant source of signal events in regions

[10] These figures are generated using private codes; however, these have been cross-checked against those of the ISASUSY package of ISAJET [30] and the two are generally consistent, exceptions being a few coding errors in ISASUSY and the latter's inclusion of some mild radiative corrections for the slepton and –ino masses which are not incorporated into the codes used here. These caveats are noteworthy since results from the output of the ISASUSY code will be used as input for the simulation work that follows. These small distinctions may cause a shift in the parameter space locations of particularly-abrupt changes in the rates due to encountered thresholds, though the gross features found in this section and in the ISASUSY-based simulation studies are in very good agreement. Finally, note that higher-order corrections to the Higgs boson –ino –ino couplings are incorporated into neither ISASUSY nor the private code. A recent study[31] indicates that these generally enhance the partial decay widths by $\mathcal{O}10\%$; enhancement to BRs may be even more. This would make rates reported in this work on the conservative low side.

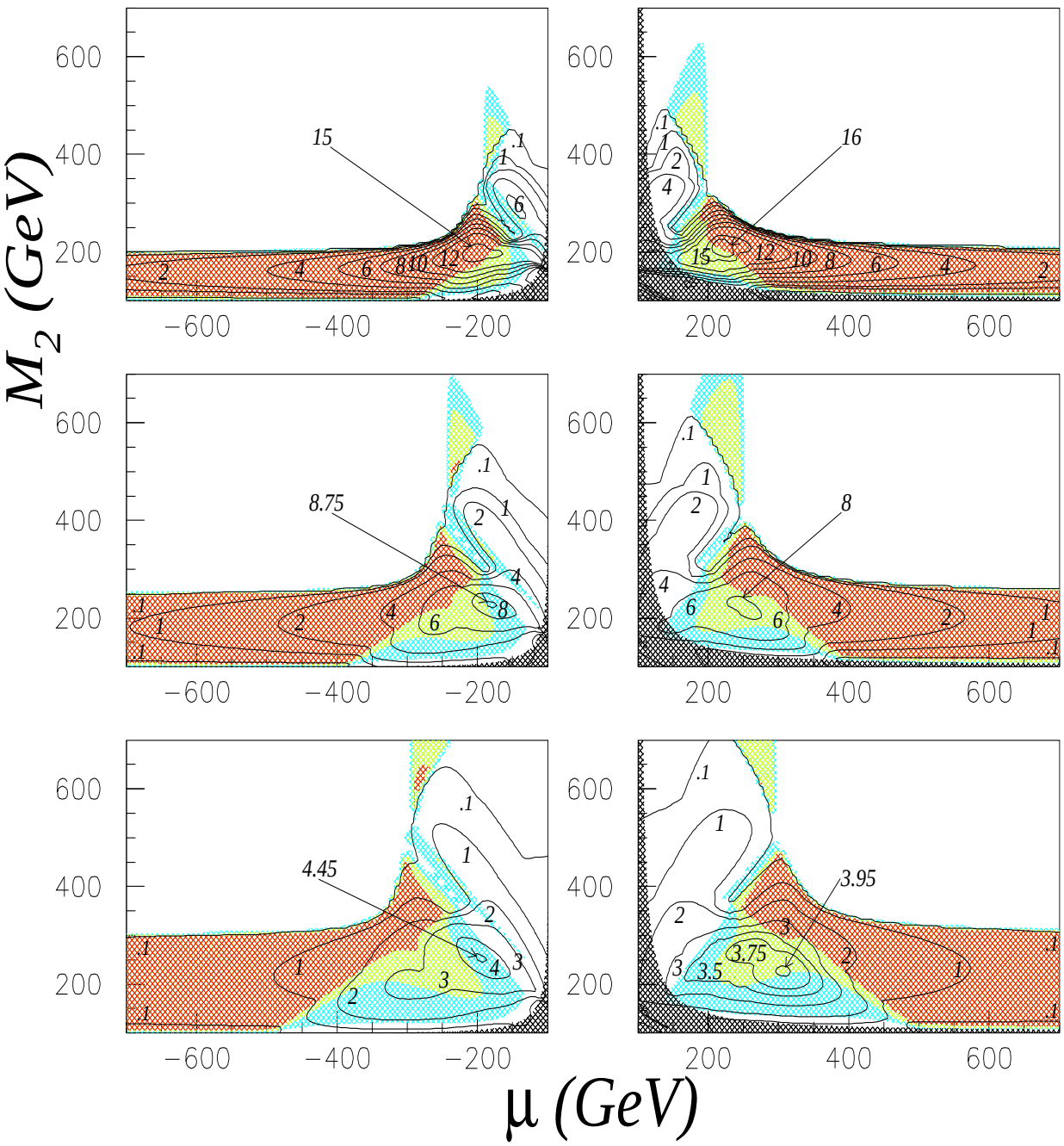

Figure 1: $\sigma(pp \to H^0, A^0) \times \mathrm{BR}(H^0, A^0 \to 4\ell N)$ (in fb), where $\ell = e^{\pm}$ or $\mu^{\pm}$ and N represents invisible final state particles, also showing where the percentage from $H^0, A^0 \to \widetilde{\chi}_2^0 \widetilde{\chi}_2^0$ is $>$ 90% (red), 50% – 90% (yellow), 10% – 50% (light blue), $<$ 10% (white), with $\tan\beta = 5$, $M_A = 400\,\mathrm{GeV}$ (top), 500 GeV (middle), 600 GeV (bottom). Optimized slepton masses (with stau inputs raised 100 GeV) are used, and with $m_t = 175\,\mathrm{GeV}$, $m_b = 4.25\,\mathrm{GeV}$, $m_{\widetilde{q}} = 1\,\mathrm{TeV}$, $m_{\widetilde{g}} = 800\,\mathrm{GeV}$, $A_\tau = A_\ell = 0$. The cross-hatch shaded areas are excluded by LEP.

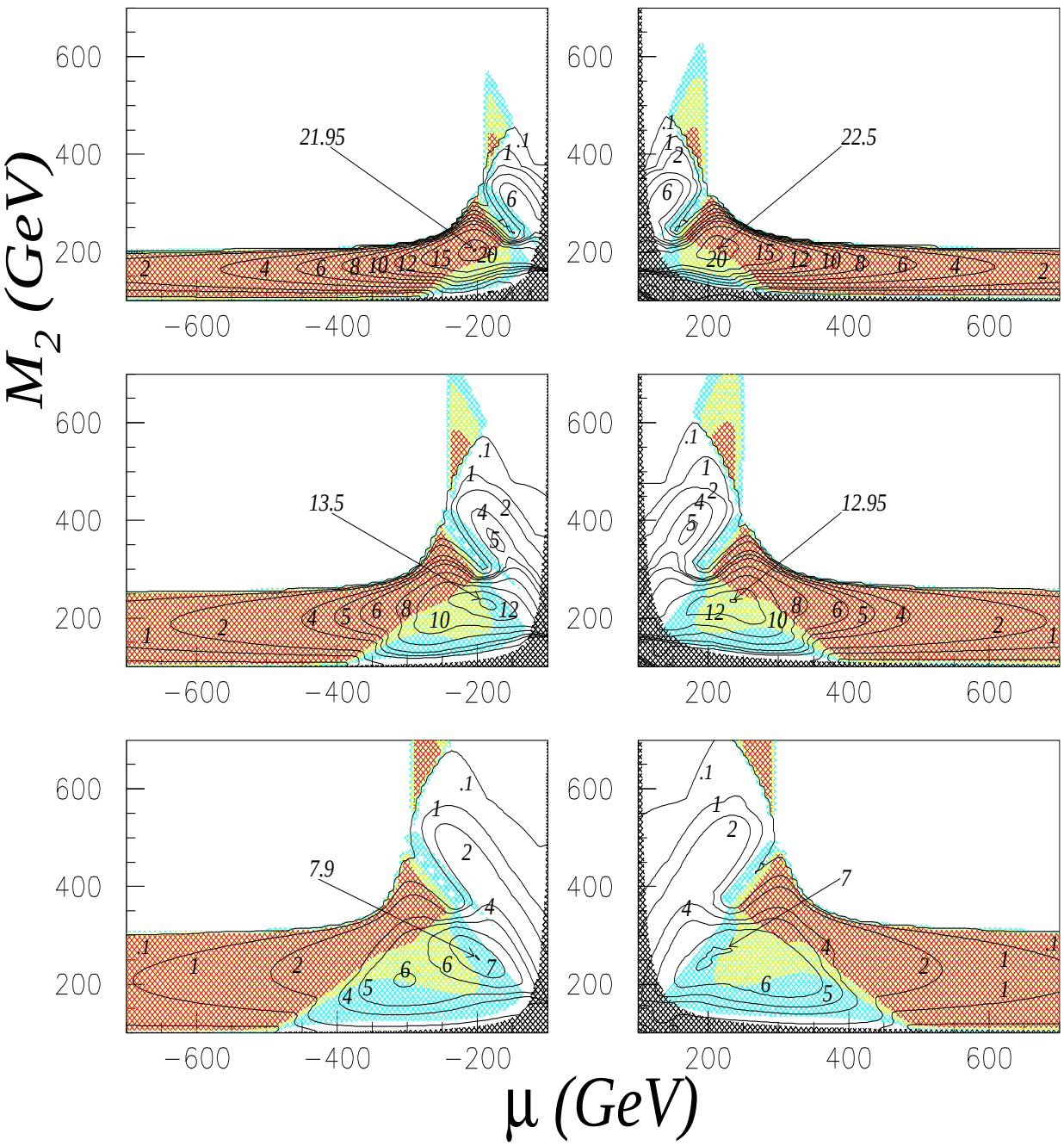

Figure 2: $\sigma(pp \to H^0, A^0) \times \mathrm{BR}(H^0, A^0 \to 4\ell N)$ (in fb), where $\ell = e^{\pm}$ or $\mu^{\pm}$ and N represents invisible final state particles, also showing where the percentage from $H^0, A^0 \to \widetilde{\chi}_2^0 \widetilde{\chi}_2^0$ is $>$ 90% (red), 50% – 90% (yellow), 10% – 50% (light blue), $<$ 10% (white), with $\tan\beta = 10$, $M_A = 400\,\mathrm{GeV}$ (top), 500 GeV (middle), 600 GeV (bottom). Optimized slepton masses (with stau inputs raised 100 GeV) are used, and with $m_t = 175\,\mathrm{GeV}$, $m_b = 4.25\,\mathrm{GeV}$, $m_{\widetilde{q}} = 1\,\mathrm{TeV}$, $m_{\widetilde{g}} = 800\,\mathrm{GeV}$, $A_\tau = A_\ell = 0$. The cross-hatch shaded areas are excluded by LEP.

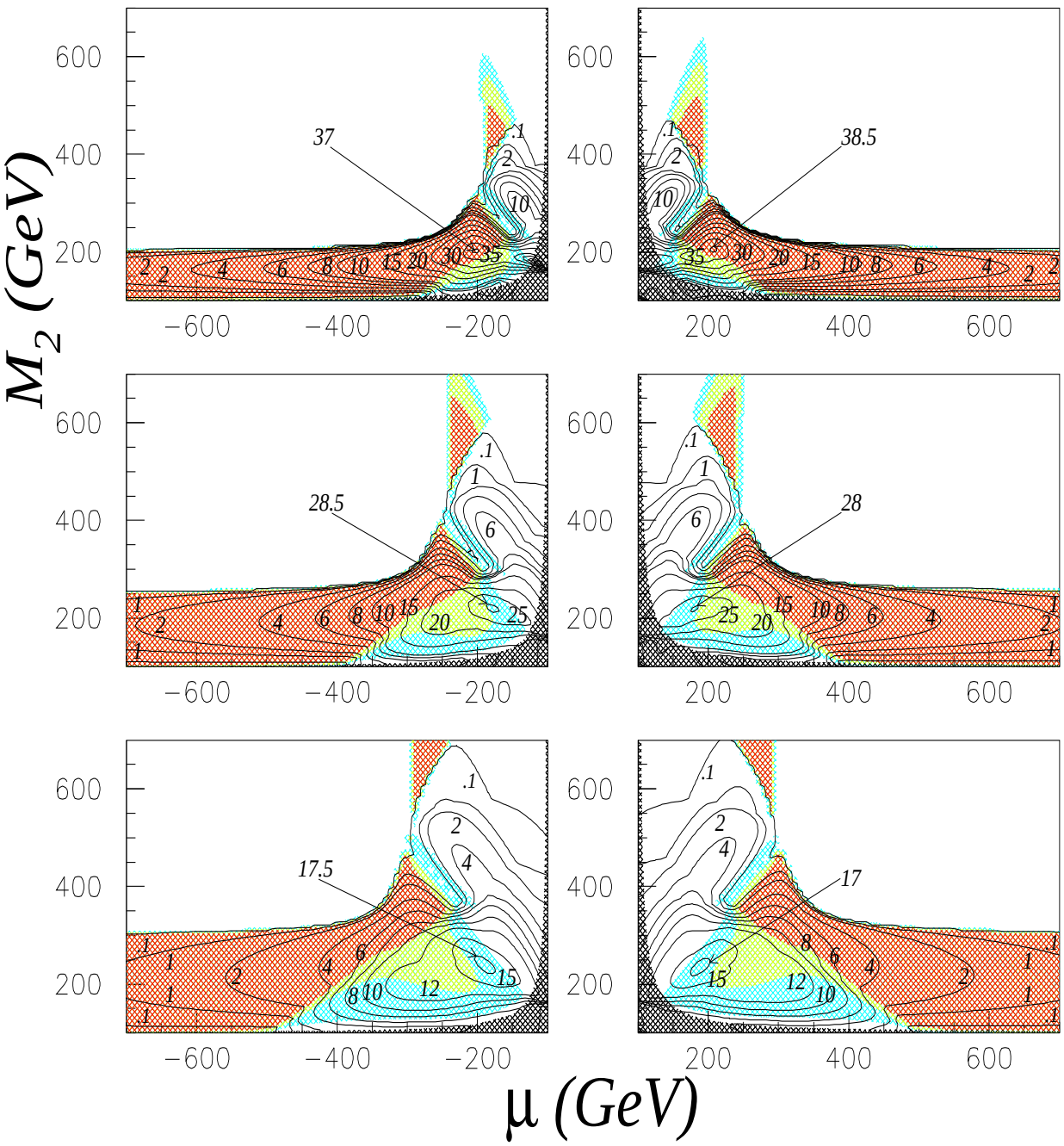

Figure 3: $\sigma(pp \to H^0, A^0) \times \mathrm{BR}(H^0, A^0 \to 4\ell N)$ (in fb), where $\ell = e^{\pm}$ or $\mu^{\pm}$ and N represents invisible final state particles, also showing where the percentage from $H^0, A^0 \to \widetilde{\chi}_2^0 \widetilde{\chi}_2^0$ is $>$ 90% (red), 50% – 90% (yellow), 10% – 50% (light blue), $<$ 10% (white), with $\tan\beta = 20$, $M_A = 400\,\mathrm{GeV}$ (top), 500 GeV (middle), 600 GeV (bottom). Optimized slepton masses (with stau inputs raised 100 GeV) are used, and with $m_t = 175\,\mathrm{GeV}$, $m_b = 4.25\,\mathrm{GeV}$, $m_{\widetilde{q}} = 1\,\mathrm{TeV}$, $m_{\widetilde{g}} = 800\,\mathrm{GeV}$, $A_\tau = A_\ell = 0$. The cross-hatch shaded areas are excluded by LEP.

with low M_2 values and moderate to high values of $|\mu|$. But for low to moderate M_2 values and low values of $|\mu|$, the dominant source of signal events shifts to the previously-neglected decays into the heavier –inos. Thus, inclusion of these neglected modes opens up an entirely new sector of the MSSM parameter space for exploration. Furthermore, the parameter space locations with the maximum number of signal events also shifts to these new sectors as the masses of the Higgs bosons rise. Therefore, the regions in MSSM parameter space wherein $\sigma(pp \to H^0, A^0) \times \mathrm{BR}(H^0, A^0 \to 4\ell N)$ processes can be utilized in the search for the heavier MSSM Higgs bosons will certainly expand substantially with inclusion of these additional decay channels.

The rates illustrated in Figs. 1–3 incorporate indirect decay modes. That is, if the Higgs boson decays into a pair of neutralinos, and then one or both of these 'primary' neutralinos decay into other neutralinos (or other sparticles or the light Higgs boson or both on- and off-mass-shell SM gauge bosons) which in turn give rise to leptons (*with no additional colored daughter particles*), then the contribution from such a decay chain is taken into account. This remains true no matter how many decays there are in the chain between the primary –ino and the $4\ell N$ final state, the only restrictions being that each decay in the chain must be a tree-level decay with at most one virtual intermediate state (so 1 to 3 decay processes are included but not 1 to 4 decays, *etc.*). (As already intimated, the intermediate state is expected to be an on- or off-mass-shell SM gauge boson or slepton, charged or neutral.) The decay modes omitted due to these restrictions are never expected to be significant. Thus, effectively all tree-level decay chains allowable within the MSSM have been taken into account. Potential contributions from literally thousands of possible decay chains are evaluated and added to the results.

Inspection of Figs. 1–3 supports selection of the following representative points in the MSSM parameter space to be employed repeatedly in this work. These are:

Point 1. $M_A = 500\,\mathrm{GeV}$, $\tan\beta = 20$, $M_1 = 90\,\mathrm{GeV}$, $M_2 = 180\,\mathrm{GeV}$, $\mu = -500\,\mathrm{GeV}$, $m_{\widetilde{\ell}_{soft}} = m_{\widetilde{\tau}_{soft}} = 250\,\mathrm{GeV}$, $m_{\widetilde{g}} = m_{\widetilde{q}} = 1000\,\mathrm{GeV}$.

Point 2. $M_A = 600\,\mathrm{GeV}$ $\tan\beta = 35$, $M_1 = 100\,\mathrm{GeV}$ $M_2 = 200\,\mathrm{GeV}$ $\mu = -200\,\mathrm{GeV}$, $m_{\widetilde{\ell}_{soft}} = 150\,\mathrm{GeV}$, $m_{\widetilde{\tau}_{soft}} = 250\,\mathrm{GeV}$, $m_{\widetilde{g}} = 800\,\mathrm{GeV}$, $m_{\widetilde{q}} = 1000\,\mathrm{GeV}$.

(Also recall that $m_{\widetilde{\ell}_{soft}} \equiv m_{\widetilde{\ell}_R} = m_{\widetilde{\ell}_L}$ and $A_\tau = A_\ell = 0$.) Point 1 represents a case where most of the signal events result from $H^0, A^0 \to \widetilde{\chi}_2^0\widetilde{\chi}_2^0$ decays[11], whereas Point 2 is a case where decays including heavier -inos make the dominant contribution. Here $\tan\beta$ has been set fairly high to enhance rates, as Figs. 1–3 suggest.

In Fig. 4, the parameter values of Point 1 (left plot) and Point 2 (right plot) are adopted, save that the parameters M_A and $\tan\beta$ are allowed to vary, generating plots in the M_A *vs.* $\tan\beta$ plane. Color shading on the left-side plot clearly shows that the $\widetilde{\chi}_2^0\widetilde{\chi}_2^0$ decay modes totally dominate in the production of 4ℓ signal events for this choice of M_2, μ -ino inputs out to $M_A \simeq 700\,\mathrm{GeV}$. Similarly, the right-side plot shows that for the –ino inputs of Point 2 the

[11] This choice of parameters, including the degenerate soft selectron, smuon and stau inputs, also corresponds to one of the choices adopted in [9].

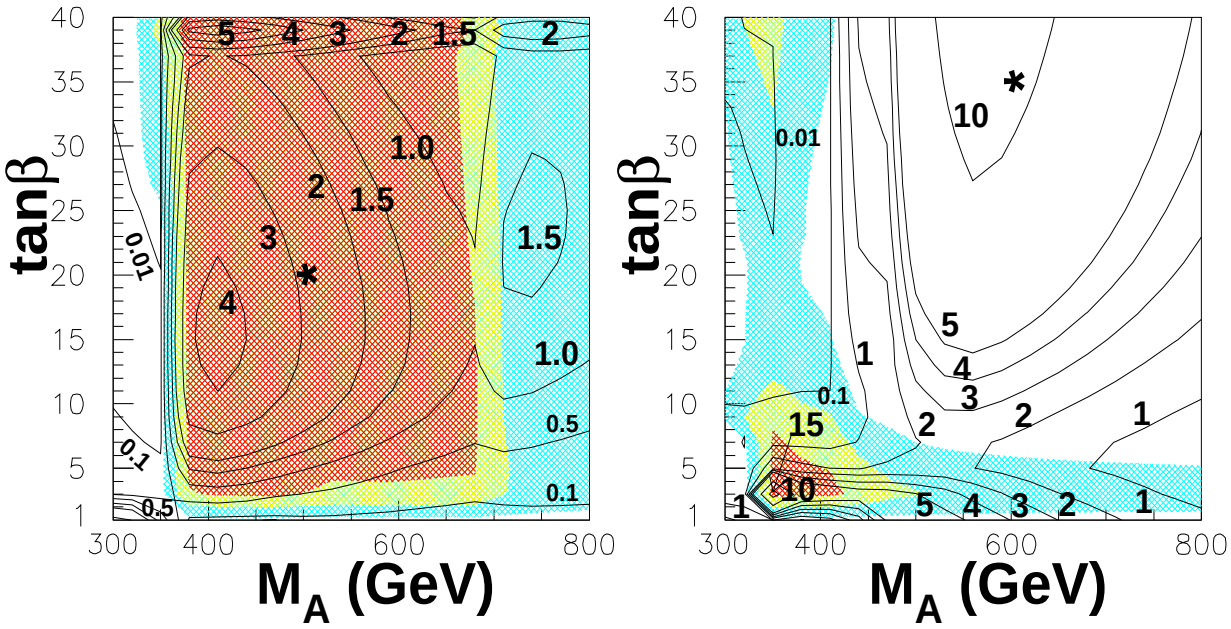

Figure 4: $\sigma(pp \to H^0, A^0) \times \mathrm{BR}(H^0, A^0 \to 4\ell N)$ (in fb), where $\ell = e^{\pm}$ or $\mu^{\pm}$ and N represents invisible final state particles for Point 1 (left side): $M_1 = 90\,\mathrm{GeV}$, $M_2 = 180\,\mathrm{GeV}$, $\mu = -500\,\mathrm{GeV}$, $m_{\widetilde{\ell}_{soft}} = m_{\widetilde{\tau}_{soft}} = 250\,\mathrm{GeV}$, $m_{\widetilde{g}} = m_{\widetilde{q}} = 1000\,\mathrm{GeV}$; and Point 2 (right side): $M_1 = 100\,\mathrm{GeV}$, $M_2 = 200\,\mathrm{GeV}$, $\mu = -200\,\mathrm{GeV}$, $m_{\widetilde{\ell}_{soft}}/m_{\widetilde{\tau}_{soft}} = 150/250\,\mathrm{GeV}$, $m_{\widetilde{g}}/m_{\widetilde{q}} = 800/1000\,\mathrm{GeV}$. Color coding as in Figs. 1–3.

previously neglected decay modes to heavier –inos dominate, save for a relatively small region around $M_A \sim$ 350-450 GeV and $\tan\beta \sim$ 2-10. Color coding as in Figs. 1–3.

It will be noteworthy to compare the declines in raw rates with increasing M_A and decreasing $\tan\beta$ shown here to the corresponding M_A *vs.* $\tan\beta$ discovery region plots based on detailed simulation analyses presented in the analysis section to follow.

Fig. 5 illustrates how results depend on the slepton mass(es). In the upper plot, showing the overall rate, $\sigma(pp \to H^0, A^0) \times \mathrm{BR}(H^0, A^0 \to 4\ell N)$, as a function of $m_{\widetilde{\ell}_{soft}} \equiv m_{\widetilde{\ell}_{L,R}}$, one generally sees the naively expected decline in the rate as $m_{\widetilde{\ell}_{soft}}$ increases. If the –inos decay through on- or off-mass-shell sleptons, then the decay products always include leptons (and usually charged leptons). However, as the sleptons become heavier (first becoming kinematically inaccessible as on-mass-shell intermediates and then growing increasingly disfavored as off-mass-shell intermediates), the EW gauge bosons become the dominant intermediates, in which case a large fraction of the time the decay products will be non-leptons, and so the BR to the 4ℓ final state drops. The plot though also reveals an often far more complex dependence on $m_{\widetilde{\ell}_{soft}}$, with rapid oscillations in the rate possible for modest changes in $m_{\widetilde{\ell}_{soft}}$.

Note again that Point 1, drawn in red in Fig. 5, represents a case where most of the signal events result from $H^0, A^0 \to \widetilde{\chi}_2^0\widetilde{\chi}_2^0$ decays, whereas Point 2, drawn in blue, is a case where decays including heavier –inos make the dominant contribution. This is made clear by the lower plot where the percentage of the inclusive rate from $\widetilde{\chi}_2^0\widetilde{\chi}_2^0$ decays is plotted *vs.* $m_{\widetilde{\ell}_{soft}}$. In Fig. 5, the slepton mass is varied. But later in this work the value of $m_{\widetilde{\ell}_{soft}}$ will be fixed at

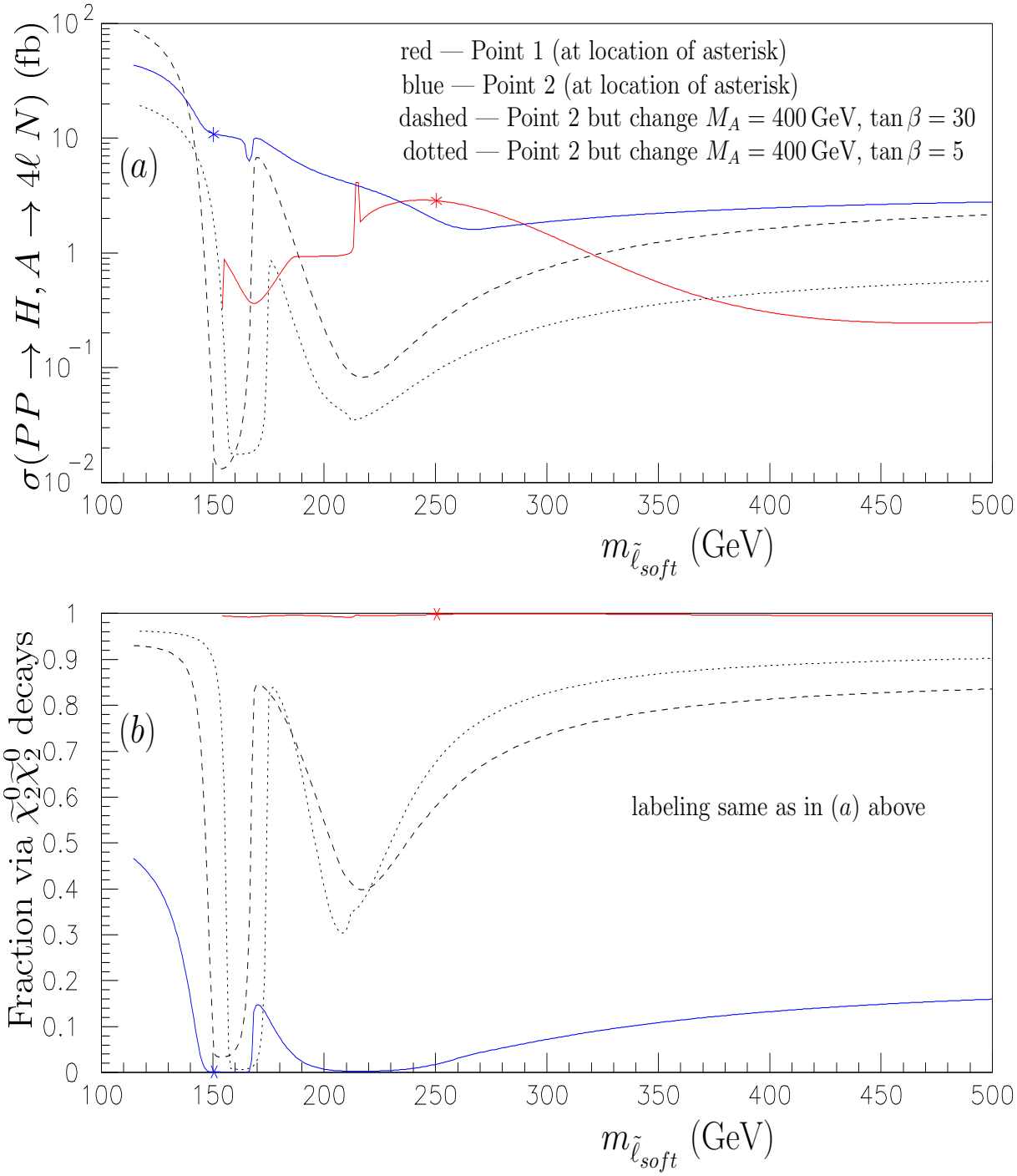

Figure 5: Dependence on slepton mass. (*a*) $\sigma(pp \to H^0, A^0) \times \text{BR}(H^0, A^0 \to 4\ell N)$ (in fb), where $\ell = e^{\pm}$ or $\mu^{\pm}$ and N represents invisible final state particles, *vs.* $m_{\widetilde{\ell}_{soft}} \equiv m_{\widetilde{\ell}_{L,R}}$ for MSSM parameter Point 1 (red) and Point 2 (blue) as well as some variations based on Point 2 (black). Asterisks mark the $m_{\widetilde{\ell}_{soft}}$ values to be used for Points 1 and 2 later in this work. (*b*) percentage of the inclusive rate from $\widetilde{\chi}_2^0\widetilde{\chi}_2^0$ decays *vs.* $m_{\widetilde{\ell}_{soft}}$, with other labeling as in (*a*).

the values given earlier for Points 1. and 2. (these locations are marked by asterisks in both plots in Fig. 5). These choices are fairly optimal, especially for Point 1.

Points 1. and 2. show some interesting dependence on $m_{\widetilde{\ell}_{soft}}$. This dependence can be made more acute though by adjusting the input parameters. For instance, the black dotted and dashed curves in Fig. 5 result from lowering the M_A value of Point 2 to 400 GeV and changing $\tan\beta$ from 35 to 5 and 30, respectively. Then not only does the inclusive rate undergo rapid variation with $m_{\widetilde{\ell}_{soft}}$, but the percentage of the inclusive rate from $\widetilde{\chi}_2^0\widetilde{\chi}_2^0$ decays fluctuates rapidly as well. Points 1. and 2. were selected for further analysis later in this work in part because the results are not strongly affected by a small shift in the value of $m_{\widetilde{\ell}_{soft}}$. However, apparently this is not true for all points in MSSM parameter space.

Finally, notice that the overall normalization of both processes $gg \to H^0, A^0$ and $b\bar{b} \to H^0, A^0$ is of $2 \to 1$ lowest-order[12]. Each of these gluon- and quark-fusion partonic contributions is separately convoluted with an empirical set of PDFs (CTEQ 6M [34] in this case) to obtain predictions at the proton-proton level, for which the total center-of-mass energy is $\sqrt{s} = 14\,\text{TeV}$. The cross-section thus defined is computed using the MSSM implementation [35] of the HERWIG program [36] (as available in Version 6.5 [37], with the exception of the choices $m_t = 175\,\text{GeV}$ and $m_b = 4.25\,\text{GeV}$ for the top and bottom quark masses) and the MSSM input information produced by ISASUSY (through the ISAWIG [38] and HDECAY [41] interfaces). Sometimes a Higgs boson will be produced in association with jets, and thus, as discussed in Ref. [32], what percentage of the time a Higgs boson is produced with hadronic activity passing jet selection criteria (as will be applied in the analysis section) is (possibly) sensitive to the type of emulation ($2 \to 1$ or $2 \to 3$) being employed. Note though that in Figs. 1–4 colored fermions are not allowed in the –ino decay chains. This is in fact inconsistent and leads to an over-(under-)estimate of the hadronically-quiet (inclusive, allowing jets) 4ℓ rates (the under-estimation of the inclusive rates is expected to be modest due to the price of extra BRs in the decay chains of the neglected channels). To attempt to correct for this by factoring in results from the simulation runs might obscure what is meant by 'raw' rates, so this minor inconsistency is simply tolerated in these estimates.

2.3 Signal-to-background rates

The signal, taken here to be events resulting from heavy MSSM Higgs bosons decaying into –ino pairs, is not the only relevant quantity in this analysis that depends on the position in the MSSM parameter space — backgrounds from other MSSM processes will also vary from point to point. Fig. 1 of [27] shows the competing processes for –ino pair-production via Higgs boson decays[13]: 'direct' –ino production (*i.e.*, *via* a s-channel gauge boson) and –inos produced in 'cascade' decays of squarks and gluinos. The latter is considered in some detail in

[12]There is an alternative $2 \to 3$ approach based on MC implementation of $gg/q\bar{q} \to b\bar{b}H^0, b\bar{b}A^0$ diagrams. The results of these two approaches have been compared and contrasted in Ref. [32]. A full MC implementation for the $2 \to 3$ approach based on $gg \to ggH^0, ggA^0$ and related modes (eventually yielding two jets in the final state alongside H^0 or A^0) [33]) is as-of-yet unavailable though in public event generators. It is therefore more consistent to solely employ *complete* $2 \to 1$ emulations and not *incomplete* $2 \to 3$ ones.

[13]One could also consider signals from Higgs boson decays to other sparticles, especially sleptons. This was discussed in [39], which demonstrated that the heavier MSSM Higgs boson decays to sleptons only have sufficient BRs for low values of $\tan\beta$ ($\lesssim 3$).

[27], but will be removed from consideration here by making the assumption throughout this work that gluinos and squarks are heavy (*circa* 1 TeV). However, since the signal depends on them, (all) the –inos cannot be made heavy[14], and the masses of the EW gauge bosons are known, so the direct channel background cannot be easily removed by restricting the analysis to some subset of the parameter space by means of such a straight-forward assumption.

In fact, the location in the parameter space where the raw signal rate is largest sometimes differs from that where the ratio of the signal to the leading background from direct –ino production is largest. For instance, the plot in Fig. 2 ($\tan\beta = 10$) for $M_A = 600\,\text{GeV}$ shows a maximum in the inclusive rate at approximately $(\mu, M_2) = (-200\,\text{GeV},\ 250\,\text{GeV})$. On the other hand, the signal-to-background ratio (S/B) is largest at $\approx (-250\,\text{GeV},\ 500\,\text{GeV})$. The production cross-section for the Higgs bosons is the same at both points. Thus, to understand why the two locations differ so much the BR($H^0, A^0 \to 4\ell N$) and the direct –ino production $\times$ BR(-inos $\to 4\ell N$) need to be studied. The former drops from ∼6% to ∼2% in moving from the inclusive rate maximum to the S/B maximum (thus cutting the overall signal rate by a factor of 3). The background at the inclusive rate maximum is mostly $\widetilde{\chi}_2^0\widetilde{\chi}_3^0$, $\widetilde{\chi}_3^0\widetilde{\chi}_4^0$ and $\widetilde{\chi}_2^\pm\widetilde{\chi}_2^\mp$ with respective production cross-sections (and BRs into $4\ell N$ final states) of $4\times10^{-2}\,\text{pb}$ (18%), $1\times10^{-2}\,\text{pb}$ (8%) and $1\times10^{-2}\,\text{pb}$ (2%). At the point where the S/B is a maximum, these (still dominant) backgrounds rates shift to $1\times10^{-2}\,\text{pb}$ (16%), $1\times10^{-4}\,\text{pb}$ (27%) and $1\times10^{-2}\,\text{pb}$ (2%), respectively. So the $\widetilde{\chi}_2^0\widetilde{\chi}_3^0$ production rate drops by a factor of 4 while $\widetilde{\chi}_3^0\widetilde{\chi}_4^0$ production almost vanishes (which is the main factor), mostly because of increased phase space suppression due to larger –ino masses: $m_{\widetilde{\chi}_2^0}(m_{\widetilde{\chi}_3^0})[m_{\widetilde{\chi}_4^0}]\{m_{\widetilde{\chi}_2^\pm}\}$ changes from 118(180)[212]{289} GeV at the rate maximum to 219(257)[273]{515} GeV at the S/B maximum. The result is that the overall background rate drops by a factor of 5. In short, the S/B improves because the direct –ino pair-production cross-section falls more rapidly than the signal BR into $4\ell N$ final states. Analogous plots to those in Figs. 1–3 studying the S/B variation across the parameter space are not presented. Instead, discovery regions for selected –ino input parameter sets will be given in Sect. 4. While favorable MSSM points have been chosen for the simulation analyses, they were not selected to maximize the S/B. Therefore, this channel may work even better at points other than those analysed in detail herein.

3 mSUGRA parameter space

Augmenting the general MSSM with additional assumptions about the unification of SUSY inputs at a very high mass scale yields the more restrictive 'mSUGRA' models. Here the number of free input parameters is much reduced (hence the popularity of such scenarios for phenomenological analyses), with said free parameters generally set as $\tan\beta$, a universal gaugino mass defined at the Grand Unification Theory (GUT) scale ($M_{1/2}$), a universal GUT-level scalar mass (M_0), a universal GUT-level trilinear scalar mass term (A_0), and the sign of μ (henceforth, sgn(μ)). As already noted, the signal has a strong preference for low values of $|\mu|$. Yet in mSUGRA scenarios, $|\mu|$ is not a free parameter, as it is closely tied to the masses of the scalar Higgs bosons *via* the M_0 input. An earlier study of charged Higgs boson decays into

[14]The sleptons also cannot be made arbitrarily heavy. Direct slepton pair-production, as studied in [40], will *generally* lead to dilepton final states rather than the 4ℓ final state desired here. The smaller contributions from these processes are included in the analyses to follow.

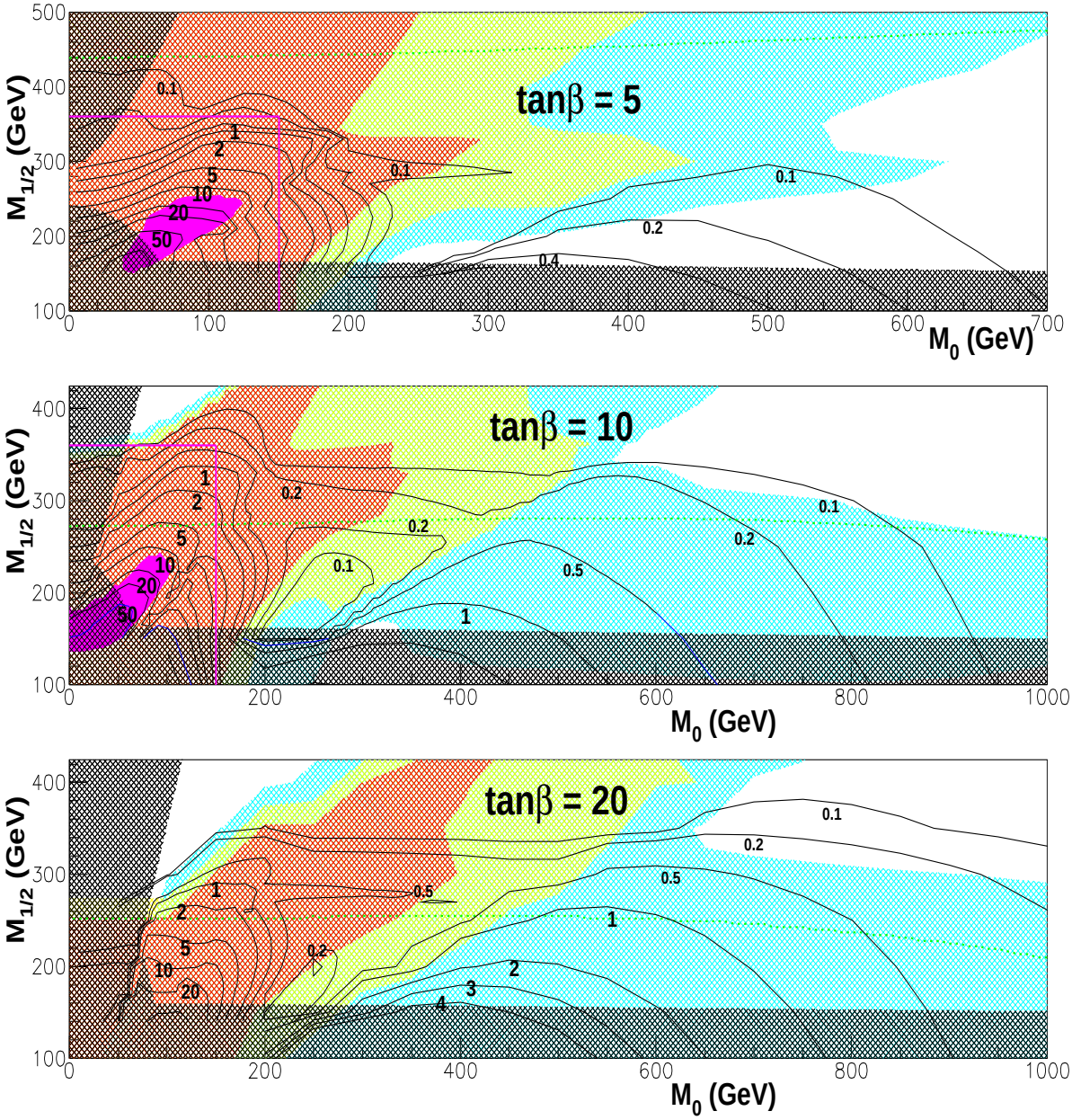

Figure 6: $\sigma(pp \to H^0, A^0) \times \mathrm{BR}(H^0, A^0 \to 4\ell N)$ (in fb), where $\ell = e^{\pm}$ or $\mu^{\pm}$ and N represents invisible final state particles for $\tan\beta = 5, 10, 20$ in the mSUGRA M_0 *vs.* $M_{1/2}$ plane, with $\mathrm{sgn}(\mu) = +1$ and $A_0 = 0$. Colors depict the percentage of events stemming from $H^0, A^0 \to \widetilde{\chi}_2^0\widetilde{\chi}_2^0 > 90\%$ (red), $50\% - 90\%$ (yellow), $10\% - 50\%$ (light blue), $< 10\%$ (white). The dark shaded regions are excluded by theoretical considerations or LEP measurements (save constraints from LEP Higgs-strahlung which roughly reach up to the dashed green curves with considerable uncertainty — see text). Also shown in purple are the CMS TDR (Fig. 11.32) 5σ discovery regions (assuming $L_{int} = 30\,\mathrm{fb}^{-1}$) for $H^0, A^0 \to \widetilde{\chi}_2^0\widetilde{\chi}_2^0$. The solid purple lines show the extent of the plots in Fig. 11.32.

a neutralino and a chargino [20] demonstrated that this was sufficient to preclude detection of a 3ℓ + top-quark signal from such processes over the entire reach of the unexcluded mSUGRA parameter space. Here, with the heavier neutral MSSM Higgs bosons, the situation is not so discouraging. Fig. 6 shows the values for $\sigma(pp \to H^0, A^0) \times \mathrm{BR}(H^0, A^0 \to 4\ell N)$ obtained for $\tan\beta = 5, 10, 20$ and $\mu > 0$. Two disconnected regions of unexcluded parameter space appear where the expected number of events (for $100\,\mathrm{fb}^{-1}$ of integrated luminosity) is in the tens to hundreds (or even thousands). Interestingly, one of these (which includes discovery regions depicted in the CSM TDR [14][15]) is where $\widetilde{\chi}_2^0\widetilde{\chi}_2^0$ is the dominant source of 4ℓ events while the other is where decays of the heavier –inos dominate. For $\tan\beta = 5$, rates in the $\widetilde{\chi}_2^0\widetilde{\chi}_2^0$ region are much larger than in the heavier –inos region. However, for $\tan\beta = 20$, rates in the two regions become more comparable.

Also shown as solid purple zones on the $\tan\beta = 5$ and $\tan\beta = 10$ plots are 5σ discovery regions from the CMS TDR (Fig. 11.32) [14]. These CMS TDR discovery regions assume an integrated luminosity of just $30\,\mathrm{fb}^{-1}$, and thus would have certainly been considerably larger if a base luminosity of $100\,\mathrm{fb}^{-1}$ was used instead. This CMS TDR analysis was at a technical level comparable to that in this work, *but only considered MSSM Higgs boson decays into* $\widetilde{\chi}_2^0\widetilde{\chi}_2^0$ *pairs*. Thus, the CMS TDR analysis would not pick up the region where heavier –ino decays dominate (in fact the plots in Fig. 11.32 in the CMS TDR only showed the regions delineated by the solid purple lines in Fig. 6). Given that the somewhat lower rates of the higher M_0, heavier –ino decays-dominated region may be compensated by assuming a larger integrated luminosity, as well as perhaps finding a higher selection efficiency due to harder daughter leptons, it is difficult to infer from the CMS TDR 5σ $30\,\mathrm{fb}^{-1}$ discovery regions whether or not disjoint discovery regions may develop in this novel region of the parameter space. This is currently under investigation [15].

The excluded regions shown in Fig. 6 merit some explanation. Note that in each plot the discovery region from the CMS TDR cuts into the excluded region, whereas in Fig. 11.32 of the CMS TDR they do not touch the (more limited) excluded regions shown. This is mainly because the excluded regions in Fig. 11.32 of the CMS TDR only mark off regions where the $\widetilde{\chi}_1^0$ is not the LSP (because the mass of the lighter stau is lower — this removes the upper left corner of the plots) and where EWSB is not obtained (along the horizontal axis), while ignoring other experimental constaints — such as the lower limit on the lighter chargino's mass from the LEP experiments. Such additional experimental constraints are included, for instance, in the excluded regions shown in Fig. 20-1 of the ATLAS TDR [16] [16]. These experimental constraints have been updated to represent the final limits from the LEP experiments, accounting for the gross differences between the excluded regions depicted

[15]Note: virtually all mSUGRA parameter space plots in the TDR showing excluded regions are for $\tan\beta = 10$; the exceptions being the $\tan\beta = 5$ plot in Fig. 11.32 and the $\tan\beta = 35$ plots in Figs. 13.12 & 13.13; and the $\tan\beta = 35$ plots seem to inaccurately have the $\tan\beta = 10$ exclusion zones. These latter plots and others in Chapter 13 do show a chargino lower mass limit (green dotdashed curve) and other supercollider experimental bounds which are more consistent with the excluded regions shown in the ATLAS TDR (and in the present work).

[16]Note: virtually all mSUGRA parameter space plots in the TDR showing excluded regions are for $\tan\beta = 10$ and for (the now ruled-out) $\tan\beta = 2$.

in the ATLAS TDR and those in the present work[17]. Somewhat crude[18] estimates for the regions excluded by the LEP searches for MSSM Higgs bosons are indicated separately by the dashed green lines based on the empirical formula developed by Djouadi, Drees and Kneur [18]. Finally, it must be emphasized that constraints from lower-energy experiments (in particular from $b \to s\gamma$) and from cosmological considerations (such as LSP dark matter annihilation rates) are *not* herein considered. In the far more restricted parameter domain of mSUGRA models it is more difficult to circumvent such constraints, and they can exclude considerable portions of the allowed parameter space shown in the figures (for further details, see [19]).

As was done with the general MSSM parameter space, Fig. 5 enables selection of a couple of representative mSUGRA points for simulation studies. These are:

Point A. $M_0 = 125\,\text{GeV}$, $M_{1/2} = 165\,\text{GeV}$, $\tan\beta = 20$, $\text{sgn}(\mu) = +1$, $A_0 = 0$.

Point B. $M_0 = 400\,\text{GeV}$, $M_{1/2} = 165\,\text{GeV}$, $\tan\beta = 20$, $\text{sgn}(\mu) = +1$, $A_0 = 0$.

Point A is dominated by $H^0, A^0 \to \widetilde{\chi}_2^0\widetilde{\chi}_2^0 \to 4\ell$ decays (which account for more than 99% of the inclusive signal event rate before cuts) while in Point B the corresponding rates are below 30% (the largest signal event channel is now $H^0, A^0 \to \widetilde{\chi}_1^\pm\widetilde{\chi}_2^\mp \to 4\ell$, yielding over 50% of the events, with significant contributions from $H^0, A^0 \to \widetilde{\chi}_2^0\widetilde{\chi}_2^0, \widetilde{\chi}_2^0\widetilde{\chi}_3^0, \widetilde{\chi}_2^0\widetilde{\chi}_4^0 \to 4\ell$). Full MC and detector simulations for Points A and B will be presented in the next section. These will show that $4\ell N$ signals remain visible in the mSUGRA parameter space, at least at these points.

4 Simulation analyses

The HERWIG 6.5 [37] MC package (which obtains its MSSM input information from ISASUSY [30] through the ISAWIG [38] and HDECAY [41] interfaces) is employed coupled with private programs simulating a typical LHC detector environment (these codes have been checked against results in the literature). The CTEQ 6M [34] set of PDFs is used and top and bottom quark masses are set to $m_t = 175\,\text{GeV}$ and $m_b = 4.25\,\text{GeV}$, respectively.

Four-lepton events are first selected according to these criteria:

- Events have exactly four leptons, $\ell = e$ or μ, irrespective of their individual charges, meeting the following criteria:

[17] Raising the lower bound on the chargino mass from the *circa* 1998 [17] LEP-1.5-era $\sim$65 GeV to $\sim$100 GeV raises the approximately horizontal boundary for higher M_0 values, while the rise of the bounds for the slepton masses from $\sim$45 GeV to $m_{\widetilde{e}_1}, m_{\widetilde{\mu}_1}, m_{\widetilde{\tau}_1} \simeq 99\,\text{GeV}, 91\,\text{GeV}, 85\,\text{GeV}$ adds the quarter-circle-like bite seen in the lower-left corner of the $\tan\beta = 10$ plot in Fig. 6 (which is absent in the ATLAS TDR plots).

[18] For reasons detailed in [18], foremost among which is the uncertainty in the calculation of M_h. Herein the Higgs boson mass formulæ of ISAJET [30] and [12] are employed. Results here are roughly consistent with Figs. 1 & 2 of [18] (2006 paper). Note that in the case of mSUGRA, unlike in the general MSSM examples in the current work, the stop and other squark parameters — which make the main contributions to the quite significant radiative corrections to M_h — are determined from the few mSUGRA inputs without the need to set values by hand for assorted soft SUSY-breaking masses. Certainly, in mSUGRA, the LEP bounds on light Higgs boson production are strongly-tied to rates for heavy Higgs boson to sparticle decay channels, though this correlation will not be intensively examined in this work.

Each lepton must have $|\eta^\ell| < 2.4$ and $E_T^\ell > 7,4$ GeV for e, μ (see ATLAS TDR [16]).
Each lepton must be isolated. The isolation criterion demands there be no tracks (of charged particles) with $p_T > 1.5\,\mathrm{GeV}$ in a cone of $r = 0.3$ radians around a specific lepton, and also that the energy deposited in the electromagnetic calorimeter be less than 3 GeV for $0.05\,\mathrm{radians} < r < 0.3\,\mathrm{radians}$.
Aside from the isolation demands, no restrictions are placed at this stage on the amount of hadronic activity or the number of reconstructed jets in an event.

Further,

- Events must consist of two opposite-sign, same-flavor lepton pairs.

Events thus identified as candidate signal events are then subjected to the following cuts:

- Z^0-veto: no opposite-charge same-flavor lepton pairs may reconstruct $M_Z \pm 10$ GeV.
- restrict E_T^ℓ: all leptons must finally have $20\,\mathrm{GeV} < E_T^\ell < 80\,\mathrm{GeV}$.
- restrict missing transverse energy, E_T^{miss}: events must have $20\,\mathrm{GeV} < E_T^{\mathrm{miss}} < 130\,\mathrm{GeV}$.
- cap E_T^{jet}: all jets must have $E_T^{\mathrm{jet}} < 50\,\mathrm{GeV}$.
  Jets are reconstructed using a UA1-like iterative (*i.e.*, with splitting and merging, see Ref. [42] for a description of the procedure) cone algorithm with fixed size 0.5, wherein charged tracks are collected at $E_T > 1\,\mathrm{GeV}$ and $|\eta| < 2.4$ and each reconstructed jet is required to have $E_T^{\mathrm{jet}} > 20\,\mathrm{GeV}$.

Lastly, application of an additional cut on the four-lepton invariant mass is investigated:

- four-lepton invariant mass (inv. m.) cut: the 4ℓ inv. m. must be $\leq 240\,\mathrm{GeV}$.

For the signal events, the upper limit for the four-lepton inv. m. will be $M_{H,A} - 2M_{\widetilde{\chi}_1^0}$, and thus its value is dependent upon the chosen point in MSSM parameter space. In the actual experiment, the value of $M_{H,A} - 2M_{\widetilde{\chi}_1^0}$ would be *a priori* unknown. So one could ask how a numerical value can be chosen for this cut? If too low a value is selected, many signal events will be lost. On the other hand, if too large a value is chosen, more events from background processes will be accepted, diluting the signal. One could envision trying an assortment of numerical values for the four-lepton inv. m. upper limit (one of which could for instance be the nominal value of 240 GeV noted above) to see which value optimized the signal relative to the backgrounds. However, here sparticle production processes are very significant backgrounds (after application of the other three cuts, only such processes and residual $Z^{0(*)}Z^{0(*)}$ events remain), which, like the signal, may well have unknown rates. Thus, strengthening this cut would lower the total number of events without indicating whether the signal to background ratio is going up or down — unless additional information is available from other studies at least somewhat restricting the location in MSSM parameter space Nature has chosen. If such information were available, this cut could indeed lead to a purer set of signal events. One could instead consider all events from MSSM processes to be the signal while the SM processes comprise the background. However, the aim of this work is to identify the heavier Higgs bosons, not merely to identify an excess attributable to SUSY.

Table 1: Relevant sparticle masses (in GeV) for specific MSSM and mSUGRA parameter points studied in the analyses.

	Point 1	Point 2	Point A	Point B
M_A	500.0	600.0	257.6	434.9
M_H	500.7	600.8	257.8	435.3
$\widetilde{\chi}_1^0$	89.7	93.9	60.4	60.8
$\widetilde{\chi}_2^0$	176.3	155.6	107.8	108.0
$\widetilde{\chi}_3^0$	506.9	211.8	237.6	232.8
$\widetilde{\chi}_4^0$	510.9	262.2	260.0	256.3
$\widetilde{\chi}_1^\pm$	176.5	153.5	106.8	106.8
$\widetilde{\chi}_2^\pm$	513.9	263.2	260.0	258.2
$m_{\widetilde{\nu}}$	241.6	135.5	154.8	407.9
$m_{\widetilde{e}_1}$	253.8	156.3	145.7	406.1
$m_{\widetilde{\mu}_1}$	252.0	154.3	145.6	406.1
$m_{\widetilde{e}_2}$	254.4	157.2	174.1	415.7
$m_{\widetilde{\mu}_2}$	256.2	159.2	174.2	415.7
$m_{\widetilde{e}_2} - m_{\widetilde{e}_1}$	0.59	0.96	28.46	9.56
$m_{\widetilde{\mu}_2} - m_{\widetilde{\mu}_1}$	4.20	4.81	28.62	9.63

Detailed results are tabulated for the aforementioned two general MSSM and two mSUGRA parameter space points. MSSM Point 1 and mSUGRA Point A have the vast majority of their 4ℓ events from $H^0, A^0 \to \widetilde{\chi}_2^0\widetilde{\chi}_2^0$, while MSSM Point 2 and mSUGRA Point B obtain most of their 4ℓ events from Higgs boson decays to heavier –ino pairs ($\widetilde{\chi}_2^0\widetilde{\chi}_3^0$, $\widetilde{\chi}_2^0\widetilde{\chi}_4^0$ $\widetilde{\chi}_3^0\widetilde{\chi}_3^0$, $\widetilde{\chi}_3^0\widetilde{\chi}_4^0$ and/or $\widetilde{\chi}_4^0\widetilde{\chi}_4^0$). The sparticle spectra[19] for these points are presented in Table 1.

4.1 MSSM benchmark points

Table 2 shows results for MSSM Point 1, a $H^0, A^0 \to \widetilde{\chi}_2^0\widetilde{\chi}_2^0$-dominated point. Note that, after cuts, signal events do make up the majority of events in the sample. The only remaining backgrounds are from direct neutralino/chargino pair-production[20] (denoted by $\widetilde{\chi}\widetilde{\chi}$), from slepton pair-production (denoted by $\widetilde{\ell}$, $\widetilde{\nu}$) and from $Z^{0(*)}Z^{0(*)}$ production. The number of events obtained from A^0 decays after cuts is about twice the number obtained from H^0 decays. This is despite the fact that the H^0 and A^0 production cross sections are the same within 1%. The ratio of A^0 to H^0 events at this point can be compared to that for inclusive rates

[19]The older ISASUSY version which inputs sparticle masses into HERWIG 6.3 lacks D-terms in the slepton masses, meaning the smuon masses in the simulation runs equate to the selectron masses given in Table 1. This has a minor effect upon the edges in the Dalitz-like 'wedgebox' plots to be shown later. See discussion in [27].

[20]Herein final states involving a sparton and a chargino/neutralino are included together with the results for $\widetilde{\chi}\widetilde{\chi}$, as designed in HERWIG, though for the points studied here the latter overwhelmingly dominate the former.

Table 2: Event rates after the successive cuts defined in the text for MSSM Point 1 (assuming an integrated luminosity of $100\,\mathrm{fb}^{-1}$).

Process	4ℓ events	$\ell^+\ell^-\ell^{(\prime)+}\ell^{(\prime)-}$	Z^0-veto	E_T^ℓ	$E_T^{\rm miss}$	$E_T^{\rm jet}$	4ℓ inv. m.
$\widetilde{q}$, $\widetilde{g}$	118	64	49	19	1	0	0
$\widetilde{\ell}$,$\widetilde{\nu}$	100	65	46	30	23	13	7
$\widetilde{\chi}\widetilde{\chi}, \widetilde{q}/\widetilde{g}\widetilde{\chi}$	34	17	13	10	5	2	1
tH^- + c.c.	0	0	0	0	0	0	0
$Z^{0(*)}Z^{0(*)}$	1733	1683	43	39	5	4	4
$t\bar{t}Z^{0(*)}$	47	23	2	1	1	0	0
$t\bar{t}h^0$	4	2	2	1	1	0	0
H^0, A^0 signal	20,32	18,31	14,26	13,25	11,22	8,17	6,13

(with no cuts) which may be calculated using the BRs obtained from ISASUSY[21]. Including all possible decay chains, ISASUSY numbers predict $A^0 : H^0 = 1.83 : 1.00$ (64.7% A^0 events). This is in reasonable agreement with $A^0 : H^0 = 1.6 : 1.0$ (61.5% A^0 events) obtained from the 4ℓ before cuts entries in the first column of Table 2. The different H^0 and A^0 event rates may then be traced back to differences in the H^0/A^0-$\widetilde{\chi}_2^0$-$\widetilde{\chi}_2^0$ couplings (as opposed to the enhancing or opening up of other H^0 decay modes, such as for instance $H^0 \to h^0h^0$). Study of the inclusive rates based on the ISASUSY BRs also confirmed that over 99% of the four-lepton signal events resulted from $H^0/A^0 \to \widetilde{\chi}_2^0\widetilde{\chi}_2^0$ decays. The percentage of $A^0 \to 4\ell$ events surviving the subsequent cuts is about 10% larger than the percentage of $H^0 \to 4\ell$ events surviving.

Fixing the –ino input parameters M_2 & μ and the slepton & squark inputs to be those of MSSM Point 1, $\tan\beta$ and M_A were then varied to map out a Higgs boson discovery region in the traditional (M_A, $\tan\beta$) plane. This is shown in red in Fig. 7, where the solid (dashed) red border delineates the discovery region assuming an integrated luminosity of $300\,\mathrm{fb}^{-1}$ ($100\,\mathrm{fb}^{-1}$). The exact criteria used for demarcating the discovery region is that there be at least 10 signal events and that the 99%-confidence-level upper limit on the background is smaller than the 99%-confidence-level lower limit on the signal plus background. Mathematically, the latter condition translates into the formula [43]:

$$N_{\rm signal} > (2.32)^2 \left[1 + \frac{2\sqrt{N_{\rm bckgrd}}}{2.32}\right] \quad , \tag{2}$$

where $N_{\rm signal}$ and $N_{\rm bckgrd}$ are the expected number of signal and background events, respectively. As with MSSM Point 1, direct neutralino/chargino pair-production, slepton pair production and SM $Z^{0(*)}Z^{0(*)}$ are the only background processes remaining after cuts (the actual number of surviving background events varies modestly with $\tan\beta$) at all points tested,

[21] These were normalized using HERWIG production cross-sections, though here this is of scant importance since the H^0 and A^0 production cross-sections are almost the same. Also, for consistency with the HERWIG simulation analysis, ISASUSY Version 7.56 was used to generate the BRs.

with slepton pair production continuing as the dominant background. Taking into account these backgrounds, 24-28 (38-45) signal events are required to meet the criteria for $100\,\mathrm{fb}^{-1}$ ($300\,\mathrm{fb}^{-1}$) of integrated luminosity, depending on the value of $\tan\beta$, if the four-lepton inv. m. cut is not employed. Adding in this last optional cut changes the required numbers to 19-22 (28-34) signal events and shifts the discovery region boundaries to those shown as blue (dashed blue) curves in Fig. 7. This places MSSM Point 1 just outside the upper M_A edge of the $100\,\mathrm{fb}^{-1}$ discovery region (whether or not the four-lepton inv. m. cut is used). Lowering M_A to 400 GeV raises the number of signal events from 25 to 36. Note that Fig. 4 (left-side plot) predicts that $H^0, A^0 \to \widetilde{\chi}_2^0\widetilde{\chi}_2^0$ decays will generate the bulk of the signal throughout the discovery region. The lower M_A edge of the discovery region closely follows where the (dominant) $\widetilde{\chi}_2^0\widetilde{\chi}_2^0$ decay becomes kinematically accessible, *i.e.*, $M_A \geq 2m_{\widetilde{\chi}_2^0}$. The A^0 contribution outweighing the H^0 contribution was found to be a general result valid for almost[22] all points in the $(M_A, \tan\beta)$-plane tested: events from A^0 equaled or outnumbered those from H^0. Note from Table 2 that MSSM Point 1 at $M_A = 500\,\mathrm{GeV}$ and $\tan\beta = 20$ yielded $A^0 : H^0 = 2.1 : 1.0$ (68% A^0 events) *after* all cuts save the four-lepton inv. m. cut (as comparison to the numbers in the preceding paragraph indicate, A^0 events tend to do slightly better at surviving the cuts, though little reason could be found for this small effect). Lowering M_A to 400 GeV shifts this ratio to $A^0 : H^0 = 3.9 : 1.0$ (81% A^0 events).

The preponderance of A^0 events is generally greatest for lower values of M_A. For $M_A \lesssim 375\,\mathrm{GeV}$, 90-100% of the signal events are from A^0. Since $M_A < M_H$ and $M_A \simeq 2m_{\widetilde{\chi}_2^0}$ this is mainly a threshold effect. The A^0 event percentage drops to around 70% when $M_A \simeq 415\,\mathrm{GeV}$. For higher M_A values inside the $100\,\mathrm{fb}^{-1}$ discovery region (outside the $100\,\mathrm{fb}^{-1}$ discovery region but inside the $300\,\mathrm{fb}^{-1}$ discovery region), this percentage ranges from ∼70% down to ∼55% (∼60% down to ∼50%), save for the upper tip where $\tan\beta \gtrsim 30$ wherein the A^0 percentage remains above 70% or even 80%.

Inclusion of the four-lepton inv. m. cut with the nominal cut-off value of 240 GeV shifts the discovery region boundaries in Fig. 7 from the red curves to the blue ones. There are slight gains for low M_A values at high and low values for $\tan\beta$; however, the high M_A edges also recede somewhat. Note also that the highest and lowest $\tan\beta$ values which fall inside the discovery region are virtually unaltered. Though the cut's effect on the expanse of the discovery region is quite modest, inclusion of this cut at included points with lower M_A values can certainly raise the signal : background. For instance, at $(M_A,\, \tan\beta) = (400\,\mathrm{GeV},\, 20)$, this ratio goes from 37 : 19 without the 4ℓ inv. m. cut to 37 : 12 with it. However, shifting M_A to 500 GeV as in MSSM Point 1 is enough to remove any advantage, as can be seen in Table 2.

Input parameters for MSSM Point 1 were also chosen to match a point studied in a previous analysis [9] — which only looked at $\widetilde{\chi}_2^0\widetilde{\chi}_2^0$ Higgs boson decays[23]. The light purple contour shown

[22]Inside of the discovery region (for $300\,\mathrm{fb}^{-1}$), a couple points along the high M_A – lower $\tan\beta$ edge were found where the rate from H^0 very slightly exceeded that from A^0.

[23]A different simulation of the quark-fusion channel involving b (anti)quarks (in the CMS note the simulation was performed using $gg \to b\bar{b}H^0, b\bar{b}A^0$) is adopted here. In addition, the MC analysis in [9] was done with PYTHIA version 5.7 [44], which only implemented an approximated treatment of the SUSY sector, while herein ISASUSY is used in conjunction with HERWIG (though intrinsic differences between the two generators in the implementation of the PS and hadronization stages should be minimal in our context). Also, the background processes tH^- + c.c., $t\bar{t}Z$ and $t\bar{t}h$, which were not emulated in [9], in this study were checked to yield no

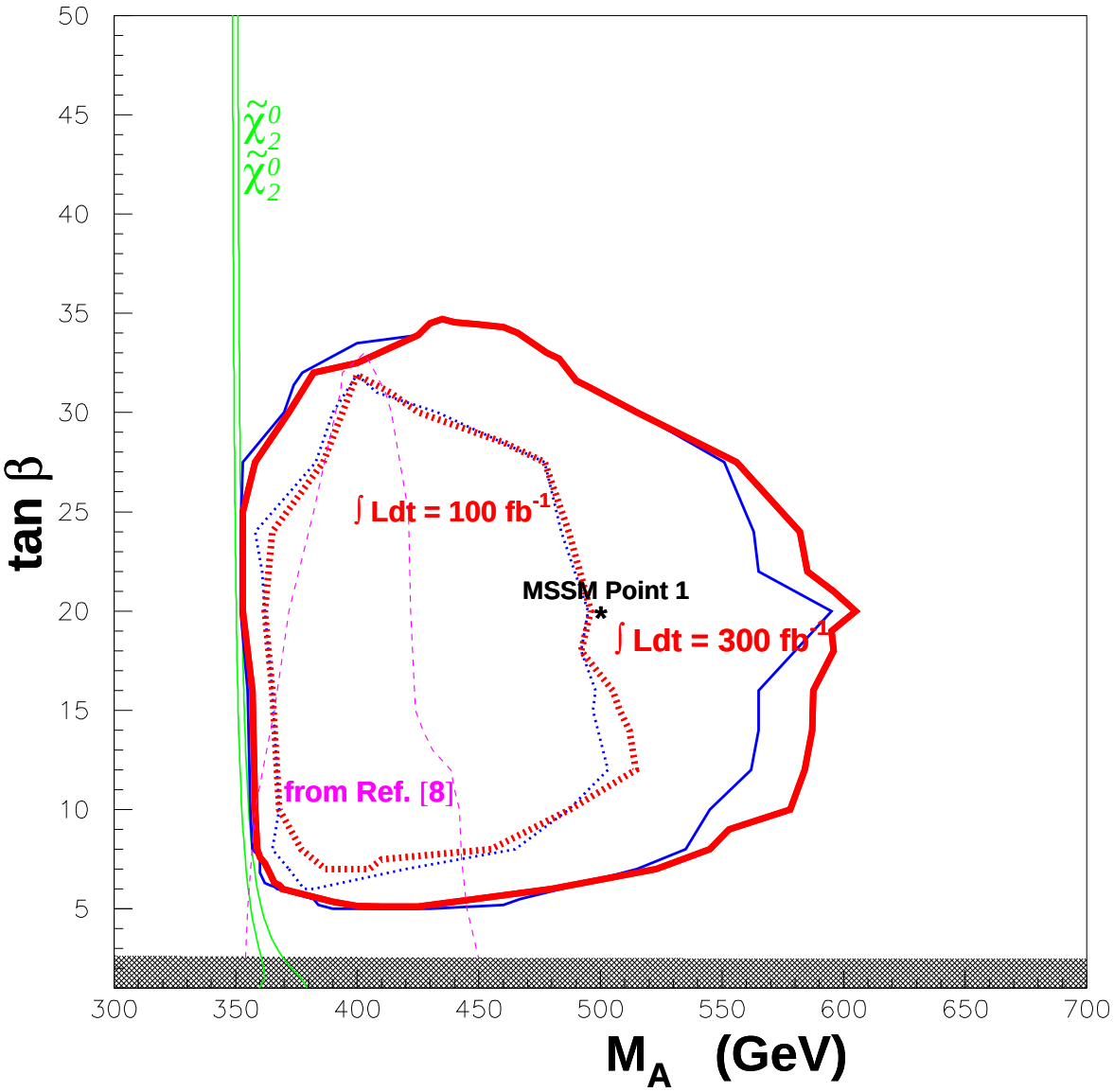

Figure 7: Discovery region in red in $(M_A, \tan\beta)$ plane for –ino/slepton parameters $\mu = -500\,\text{GeV}$, $M_2 = 180\,\text{GeV}$, $M_1 = 90\,\text{GeV}$, $m_{\widetilde{\ell}_{soft}} = m_{\widetilde{\tau}_{soft}} = 250\,\text{GeV}$ as in MSSM Point 1 (whose location is marked by a black asterisk). Here Higgs boson decays to $\widetilde{\chi}_2^0\widetilde{\chi}_2^0$ totally dominate. Solid (dashed) red border delineates the discovery region for $L_{int} = 300\,\text{fb}^{-1}$ ($100\,\text{fb}^{-1}$). The two green curves are $M_A, M_H - 2m_{\widetilde{\chi}_2^0}$. Also shown in light purple are analogous results from a previous study [9] for $100\,\text{fb}^{-1}$. The blue contours add the extra cut on the four-lepton inv. m. for the nominal cut-off value of 240 GeV.

background events throughout Fig. 7.

Table 3: Percentage of $H^0, A^0 \to 4\ell N$ events (excluding cuts) coming from various –ino channels for MSSM Point 2. (Other channels are negligible.)

$H^0 \to \widetilde{\chi}_3^0\widetilde{\chi}_4^0$	31.5%
$A^0 \to \widetilde{\chi}_4^0\widetilde{\chi}_4^0$	31.1%
$A^0 \to \widetilde{\chi}_3^0\widetilde{\chi}_4^0$	13.4%
$H^0 \to \widetilde{\chi}_4^0\widetilde{\chi}_4^0$	8.4%
$H^0 \to \widetilde{\chi}_1^\pm\widetilde{\chi}_2^\mp$	6.9%
$A^0 \to \widetilde{\chi}_1^\pm\widetilde{\chi}_2^\mp$	4.3%
$A^0 \to \widetilde{\chi}_3^0\widetilde{\chi}_3^0$	1.9%
$H^0 \to \widetilde{\chi}_3^0\widetilde{\chi}_3^0$	0.8%
$H^0 \to \widetilde{\chi}_2^+\widetilde{\chi}_2^-$	0.75%
$H^0 \to \widetilde{\chi}_2^+\widetilde{\chi}_2^-$	0.6%
all other contributions	$< 0.5\%$

in the plot is the result from this older study (see the blue contour in Fig. 19 therein). Results in the present case for the most part agree with those of that previous study, though in the current analysis the discovery region extends to somewhat higher values of M_A and dies for $\tan\beta$ values below $\sim$5. The latter is primarily due to low $\tan\beta$ strong enhancement of the $H^0(A^0)$-t-$\bar{t}$ coupling, which is proportional to $\csc\beta$ ($\cot\beta$), increasing the $H^0, A^0 \to t\bar{t}$ BRs at the expense of the –ino BRs[24]. BR($H^0 \to t\bar{t}$) (BR($A^0 \to t\bar{t}$)) rises from around 0.30 to 0.68 to 0.93 (0.51 to 0.79 to 0.96) as $\tan\beta$ runs from 6 to 4 to 2.

For MSSM Point 2, Higgs boson decays to the heavier neutralinos and charginos neglected in previous studies produce most of the signal events. Table 3 gives the percentage contributions to the signal events among the H^0, A^0 decay modes based on an inclusive rate study using BR results from ISAJET (ISASUSY) 7.58 normalized with HERWIG cross-sections. This parton-level analysis merely demands exactly four leptons in the (parton-level) final state. According to this inclusive rates study, Higgs boson decays to $\widetilde{\chi}_2^0\widetilde{\chi}_2^0$ now contribute less than one hundredth of one percent of the signal events, in stark contrast to MSSM Point 1 where such decays accounted for virtually all of the signal events. Applying all the cuts at the full event-generator level does not alter this. Said numerical results with the application of the successive cuts for MSSM Point 2 are given in Table 4.1.

Note that the four-lepton inv. m. cut, with the nominal numerical value of 240 GeV, removes about 74% of the signal events while only slightly reducing the number of background events. This clearly shows that this cut, while helpful for points with lower M_A values in Fig. 7, is quite deleterious at MSSM Point 2. Without the 4ℓ inv. m. cut, an integrated luminosity of $25\,\text{fb}^{-1}$ is sufficient to meet the discovery criteria; while with the 4ℓ inv. m. cut, an integrated luminosity of $\sim$130 fb^{-1} is required. Choosing a higher numerical cut-off would lead to a viable

[24]The partial widths for H^0 and A^0 decays to –inos also drop by roughly a factor of 2 in going from $\tan\beta = 6$ to $\tan\beta = 2$ (at $M_A = 450\,\text{GeV}$), and the $H^0 \to h^0h^0$ and $A^0 \to h^0Z^{0(*)}$ widths increase by about a factor of 2. These also lower the signal rate. On the other hand, decay widths to b-quarks and tau-leptons also drop by a bit over a factor of 2, helping the signal. These effects are overwhelmed by an almost order-of-magnitude enhancement in the H^0 and A^0 to $t\bar{t}$ decay widths.

Table 4: Event rates after successive cuts as defined in the text for MSSM Point 2 (assuming 100 fb^{-1}).

Process	4ℓ events	$\ell^+\ell^-\ell^{(\prime)+}\ell^{(\prime)-}$	Z^0-veto	E_T^{ℓ}	$E_T^{\rm miss}$	$E_T^{\rm jet}$	4ℓ inv. m.
$\widetilde{q}$, $\widetilde{g}$	817	332	197	96	21	0	0
$\widetilde{\ell}$,$\widetilde{\nu}$	12	5	4	4	2	2	2
$\widetilde{\chi}\widetilde{\chi}$, $\widetilde{q}/\widetilde{g}\widetilde{\chi}$	123	74	32	17	13	10	4
tH^- + c.c.	76	38	22	15	9	3	1
$Z^{0(*)}Z^{0(*)}$	1733	1683	43	39	5	4	4
$t\bar{t}Z^{0*}$	47	23	2	1	1	0	0
$t\bar{t}h^0$	4	1	1	1	1	0	0
H^0, A^0 signal	189,179	156,149	64,80	55,64	43,50	32,37	9,9

cut for this point; however, it may prove impossible to *a priori* decide on an appropriate value for the actual experimental analysis (see earlier discussion).

Table 4.1 gives a ratio of $A^0 \to 4\ell$ events to $H^0 \to 4\ell$ events (before additional cuts) of $A^0 : H^0 = 1 : 1.05$ (48.6% A^0 events). ISASUSY BR studies of the inclusive four-lepton event rates at this point also predict that H^0 will produce more signal events than A^0 this time, with $A^0 : H^0 = 1 : 1.36$ (42.4% A^0 events). Exact agreement between the two methods is certainly not expected, and it is at least reassuring that both predict more $H^0 \to 4\ell$ events (unlike at MSSM Point 1). The percentage of $A^0 \to 4\ell$ events surviving the subsequent cuts is again slightly larger than that for $H^0 \to 4\ell$ events (21% *vs.* 17%, excluding the four-lepton inv. m. cut). Note that the Z^0-veto takes a larger portion out of the signal event number for MSSM Point 2 than it did for MSSM Point 1, with only about 50% surviving for the former while about 80% survive for the latter. This is understandable since, for MSSM Point 1, virtually all events were from $\widetilde{\chi}_2^0\widetilde{\chi}_2^0$ pairs, and $\widetilde{\chi}_2^0$ is not heavy enough to decay to $\widetilde{\chi}_1^0$ via an on-mass-shell Z^0. For MSSM Point 2, on the other hand, a variety of heavier –inos are involved, and the mass differences between $\widetilde{\chi}_3^0$ or $\widetilde{\chi}_4^0$ and $\widetilde{\chi}_1^0$ do exceed M_Z.

Again the –ino input parameters M_2 & μ and the slepton & squark inputs are fixed, this time to be those of MSSM Point 2, and $\tan\beta$ and M_A allowed to vary to map out the Higgs boson discovery region in the (M_A, $\tan\beta$) plane (using the same criteria as in Fig. 7) shown in red in Fig. 8. As before, the solid (dashed) red border delineates the discovery region assuming an integrated luminosity of 300 fb^{-1} (100 fb^{-1}). Assuming that the four-lepton inv. m. cut is omitted, MSSM Point 2 lies firmly inside the 100 fb^{-1} discovery region (with the 15 sparticle/charged Higgs boson + 4 $Z^{0(*)}Z^{0(*)}$ event background, Relation (2) requires 26 signal events to be included in the 100 fb^{-1} discovery region, while 69 signal events are expected). Note that Fig. 4 (right-side plot) predicts that $H^0, A^0 \to \widetilde{\chi}_2^0\widetilde{\chi}_2^0$ decays will only generate a substantial number of signal events when $\tan\beta$ and M_A are small (the red and yellow zones in the plot), with decays to heavier –inos dominating elsewhere. This leads to a disjoint discovery region in Fig. 8, consisting of a smaller mainly $\widetilde{\chi}_2^0\widetilde{\chi}_2^0$-dominated portion for lower values of $\tan\beta$ and M_A and a novel larger portion at considerably higher M_A values that stretches up to $\tan\beta$ values well above 50. Note the distance between the lower M_A edge of this larger portion

of the discovery region and the curves for $M_A, M_H - 2m_{\widetilde{\chi}_2^0}$. In concurrence with the percentage contributions for MSSM Point 2 given above, the lower M_A edge of the discovery region abuts the $M_A, M_H - m_{\widetilde{\chi}_3^0} - m_{\widetilde{\chi}_4^0}$ curves (shown in green in Fig. 8), *for* $\tan\beta \gtrsim 10$. The situation for $\tan\beta \lesssim 10$ and $450\,\text{GeV} \lesssim M_A \lesssim 700\,\text{GeV}$ (in both the upper and lower disjoint portions of the discovery region) is more complicated, with $\widetilde{\chi}_2^0\widetilde{\chi}_2^0$ and several other decays making significant contributions.

The discovery region shown in Fig. 8 represents a significant extension of LHC MSSM Higgs boson detection capabilities to quite high Higgs boson masses. With $300\,\text{fb}^{-1}$ of integrated luminosity, there is some stretch of M_A values covered for almost all values of $\tan\beta$ ($1 < \tan\beta < 50$), the exception being $4 \lesssim \tan\beta \lesssim 6$. If the integrated luminosity is dropped to $100\,\text{fb}^{-1}$, the higher M_A portion of the discovery region recedes up to $\tan\beta \gtrsim$ 8-10, still lower than the $300\,\text{fb}^{-1}$ discovery regions from MSSM Higgs boson decays to third generation SM fermions found in the ATLAS [45] and other [46] simulations. The new discovery region has considerable overlap with the so-called decoupling zone, where the light MSSM Higgs boson is difficult to distinguish from the Higgs boson of the SM, and, *up to now, no signals of the other MSSM Higgs bosons were known.*

Though the number of signal events swells to over 50 (30) per $100\,\text{fb}^{-1}$ for $\tan\beta \lesssim 2$ (4), the background from –ino pair-production via EW gauge bosons is also becoming quite large, and thus more integrated luminosity is required for the excess from Higgs boson decays to meet the (2) criterion. Note how an 'excess' attributed to the Higgs boson signal could alternatively be accounted for by the MSSM background if the value of $\tan\beta$ is lowered. (Note also though that restrictions from LEP experiments exclude the most sensitive region of extremely low $\tan\beta$ values.) As in Fig. 7, the low M_A edge of the lower portion of the discovery region in Fig. 8 abuts the $M_A, M_H - 2m_{\widetilde{\chi}_2^0}$ curves.

Yet for M_A in the vicinity of 350 GeV to 450 GeV, the discovery regions in Fig. 7 and Fig. 8 resemble mirror images of each other: the former lies exclusively above $\tan\beta \simeq 5$ while the latter lies exclusively below $\tan\beta \simeq 5$. The reasons behind this stark contrast, though a bit complicated, critically depend on the different inputs to the slepton sector. In Fig. 8, for $M_A \lesssim 470\,\text{GeV}$, Higgs boson decays to other heavier -inos are kinematically inaccessible, and, for higher $\tan\beta$ values, $\widetilde{\chi}_2^0$ decays almost exclusively via sneutrinos into neutrinos and the LSP, yielding no charged leptons. This is not the case in this region of Fig. 7 — here $\widetilde{\chi}_2^0$ undergoes three-body decays via off-mass-shell sleptons and Z^{0*} with substantial BRs into charged leptons. The situation for Fig. 8 changes as $\tan\beta$ declines below ∼10 since $\widetilde{\chi}_2^0$ BRs to charged sleptons, while still much smaller than those to sneutrinos, grow beyond the percent level — sufficient to generate a low $\tan\beta$ discovery region in Fig. 8. One might expect analogous behavior in Fig. 7; however, in the low $\tan\beta$ region of Fig. 7 the partial widths $\Gamma(H^0, A^0 \to \widetilde{\chi}_2^0\widetilde{\chi}_2^0)$ are much smaller, especially for A^0, than they are in this region of Fig. 8 and decline with falling $\tan\beta$, whereas in Fig. 8 $\Gamma(H^0 \to \widetilde{\chi}_2^0\widetilde{\chi}_2^0)$ actually increases (though only moderately) as $\tan\beta$ falls. The $\widetilde{\chi}_2^0\widetilde{\chi}_2^0$ partial widths coupled with the subsequent $\widetilde{\chi}_2^0$ decays to charged leptons are large enough in the case of Fig. 8 so that the signal is not overwhelmed by the rising $\Gamma(H^0, A^0 \to t\bar{t})$ partial widths as it is in the case of Fig. 7. Also, in Fig. 8 but not in Fig. 7, as M_A increases beyond ∼450 GeV, contributions from other –ino pairs besides $\widetilde{\chi}_2^0\widetilde{\chi}_2^0$ become significant and further enhance the low $\tan\beta$ 4ℓ signal rate.

Differences in the discovery regions at very high $\tan\beta$ values are also attributable to the

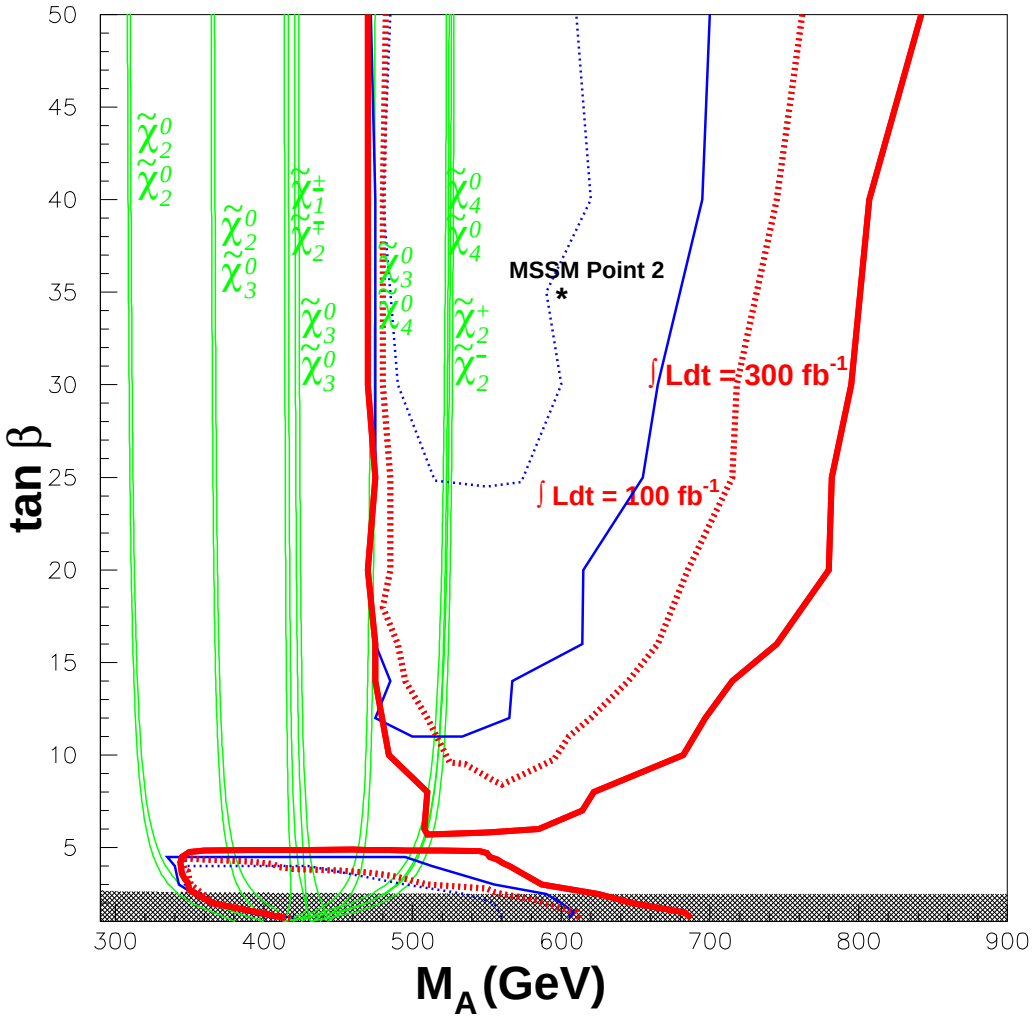

Figure 8: Discovery region in red in $(M_A, \tan\beta)$ plane for –ino/slepton parameters $\mu = -200\,\text{GeV}$, $M_2 = 200\,\text{GeV}$, $M_1 = 100\,\text{GeV}$, $m_{\widetilde{\ell}_{soft}} = 150\,\text{GeV}$, $m_{\widetilde{\tau}_{soft}} = 250\,\text{GeV}$ as in MSSM Point 2 (whose location is marked by an black asterisk). Here Higgs boson decays to a variety of higher mass –inos (see text) constitute the majority of the signal events. Solid (dashed) red border delineates the discovery region for $L_{int} = 300\,\text{fb}^{-1}$ ($100\,\text{fb}^{-1}$). The green curves are $M_A, M_H - m_{\widetilde{\chi}^0_i} m_{\widetilde{\chi}^0_j}$ and $M_A, M_H - m_{\widetilde{\chi}^\pm_k} m_{\widetilde{\chi}^\mp_2}$ $(i,j = 2,3,4;\ k = 1,2)$. The blue contours add the extra cut on the four-lepton inv. m. for the nominal cut-off value of 240 GeV.

slepton input parameters. In Fig. 8, the discovery region reaches up well beyond $\tan\beta = 50$, while in Fig. 7 the discovery region is curtailed, ending before reaching $\tan\beta = 35$. Since the soft slepton mass inputs for all three generations are degenerate for MSSM Point 1, for high $\tan\beta$ values in Fig. 7 splitting effects with the staus drive one of the physical stau masses well below the selectron and smuon masses. This leads to lots of –ino decays including tau

leptons, virtually shutting down the decays to electrons and muons. Since the soft stau mass inputs are elevated well above the other slepton inputs for MSSM Point 2, this high $\tan\beta$ cap is removed in Fig. 8.

Comments made above for MSSM Point 2 about the increased severity of the Z^0-line cut and the inappropriateness of the four-lepton inv. m. cut (with the numerical cut-off set to 240 GeV) are also applicable to points throughout the larger portion of the discovery region of Fig. 8. As can be seen from the blue curves in Fig. 8, inclusion of the 240 GeV 4ℓ inv. m. cut eliminates about half of the $300\,\text{fb}^{-1}$ discovery region and far more than half of the $100\,\text{fb}^{-1}$ region, including all points between $\tan\beta \simeq 8$ and $\tan\beta \simeq 25$ for the latter.

Also, in contrast to the discovery region of Fig. 7, in large segments of the Fig. 8 discovery region the number of signal events from H^0 decays exceed those from A^0 decays. First consider the smaller, low $\tan\beta$, portion of the disjoint discovery region. Herein, to the right of the $M_A, M_H - m_{\widetilde{\chi}_3^0} - m_{\widetilde{\chi}_4^0}$ curves (shown in green in Fig. 8), the percentage of A^0 events ranges from $\sim$30-$\sim$40% ($\sim$25-$\sim$30%) for $\tan\beta \gtrsim 2$ ($\lesssim 2$). To the left of these curves, the A^0 event percentage grows to $\sim$45-$\sim$60% for $\tan\beta \gtrsim 2$; increasing further to $\sim$70-$\sim$80% near the region's upper left tip (M_A in the vicinity of 350 GeV and $\tan\beta$ around 3 to 4.5) where the signal is dominated by Higgs-mediated $\widetilde{\chi}_2^0\widetilde{\chi}_2^0$ production.

In the novel and larger high $\tan\beta$ portion of the discovery region in Fig. 8, where the $\widetilde{\chi}_2^0\widetilde{\chi}_2^0$ contribution is minor to insignificant, the H^0 and A^0 contributions to the signal events stay within 20% of each other (with the A^0 event percentage ranging from $\sim$40-$\sim$60%) to the right of the $M_A, M_H - 2m_{\widetilde{\chi}_4^0}$ curves. In the finger-like projection between the nearly-vertical $M_A, M_H - m_{\widetilde{\chi}_3^0} - m_{\widetilde{\chi}_4^0}$ and $M_A, M_H - 2m_{\widetilde{\chi}_4^0}$ curves the A^0 percentage drops to $< 25\%$ (after cuts, excluding the 4ℓ inv. m. cut)[25], meaning that the number of events from H^0 to those from A^0 exceeds 3 to 1. The H^0 dominance in this zone stems from the H^0-$\widetilde{\chi}_3^0$-$\widetilde{\chi}_4^0$ coupling (H^0-$\widetilde{\chi}_3^0$-$\widetilde{\chi}_3^0$ coupling) being two to three times larger (smaller) than the A^0-$\widetilde{\chi}_3^0$-$\widetilde{\chi}_4^0$ coupling (A^0-$\widetilde{\chi}_3^0$-$\widetilde{\chi}_3^0$ coupling), combined with the fact that the $\widetilde{\chi}_3^0\widetilde{\chi}_4^0$ decays are about twice as likely to produce 4ℓ events as those of $\widetilde{\chi}_3^0\widetilde{\chi}_3^0$. This of course means that $\widetilde{\chi}_4^0$ has a higher leptonic BR than $\widetilde{\chi}_3^0$. This in turn is due to $\widetilde{\chi}_3^0$ decaying into $\widetilde{\chi}_1^0 Z^0$ about half the time (Z^0 gives lepton pairs $\sim$7% of the time), while $\widetilde{\chi}_4^0$ almost never decays this way, instead having larger BRs to charged sleptons [and $\widetilde{\chi}_1^\pm W^\mp$] which always [$\sim$21% of the time] yield charged lepton pairs. The situation changes quickly once the $H^0, A^0 \to \widetilde{\chi}_4^0\widetilde{\chi}_4^0, \widetilde{\chi}_2^+\widetilde{\chi}_2^-$ thresholds are (almost simultaneously, see Fig. 8) crossed, thereafter for higher M_A values the A^0 and H^0 contributions remain reasonably close to each other as already stated.

As with points in Fig. 7, direct chargino/neutralino pair-production and slepton pair-production together with $Z^{0(*)}Z^{0(*)}$ production make up most of the background surviving the cuts. Now, however, these are joined by a minor segment due to $tH^- + \text{c.c.}$ production, which depends on M_A in addition to $\tan\beta$.

Results showed $gb \to tH^- + \text{c.c.}$ could yield several events at points in the discovery region. Since the presence of a charged Higgs boson would also signal that there is an extended Higgs sector, these events could easily have been grouped with the signal rather than with the backgrounds. Clearly though the set of cuts used in this work is not designed to pick out such events. The jet cut typically removes roughly two-thirds to three-quarters of these

[25] Here are some results from specific points in this region: for $M_A = 510$ GeV and $\tan\beta = 10, 16, 25, 40$, the percentage of A^0 signal events (again, after cuts, excluding the 4ℓ inv. m. cut), is 23%, 17%, 11.5%, 21%.

events. Here though it is interesting to note that, despite the presence of a top quark, the jet cut does not remove all such events (unlike results found for squark and gluino events and four-lepton $t\bar{t}X$ events). A more effective set of cuts for tH^-, $\bar{t}H^+$ events is developed in [20], wherein substantially larger numbers of charged Higgs boson events survive the cuts therein at favorable points in the MSSM parameter space. It is also worth noting though that the reach of the discovery region (at a favorable point in the MSSM parameter space) for the $H^0, A^0 \to 4\ell$ signal as described in this work surpasses that of the charged Higgs boson discovery regions found in [20]. (or in any other previous work on Higgs boson decays to sparticles).

An aspect to be mentioned in this connection, already highlighted in Ref. [24], is the somewhat poor efficiency for the signals following the Z^0-veto, especially when combined with the fact that the $Z^{0(*)}Z^{0(*)}$ background survives the same constraint. On the one hand, a non-negligible number of events in the signal decay chains leading to $4\ell N$ final states actually proceed via (nearly) on-mass-shell Z^0 bosons, particularly for MSSM Point 2, in which the mass differences $m_{\widetilde{\chi}_i^0} - m_{\widetilde{\chi}_1^0}$ $(i = 3, 4)$ can be very large, unlike the case $m_{\widetilde{\chi}_2^0} - m_{\widetilde{\chi}_1^0}$ for MSSM Point 1 (and in previous studies limited to only $\widetilde{\chi}_2^0\widetilde{\chi}_2^0$ decay modes). On the other hand, the rather large intrinsic Z^0 width (when compared to the experimental resolution expected for di-lepton invariant masses) combined with a substantial production cross-section implies that $Z^{0(*)}Z^{0(*)}$ events will not be totally rejected by the Z^0-veto. Altogether, though, the suppression is much more dramatic for the Z^0Z^0 background than for the signal, and so this cut is retained (though the Z^0-veto will be dropped in some instances in the context of the forthcoming wedgebox analysis). Also, varying the size of the 10 GeV window around M_Z did not improve the effectiveness of this cut.

4.2 mSUGRA benchmark points

Turning attention briefly to the results within the more restrictive mSUGRA framework for SUSY-breaking, results for mSUGRA Point A and mSUGRA Point B (as defined in Sect. 3) are presented in Tables 5–6. Mass spectra for these parameter sets are given in Table 1. For mSUGRA Point A ample signal events are produced and survive the cuts to claim observation of the Higgs boson at $100\,\mathrm{fb}^{-1}$. The largest background is from direct slepton production, with direct neutralino/chargino production also contributing significantly, whereas SM backgrounds are virtually nil. Note how the E_T^{jet} cap suffices to eliminate the background from colored sparticle (squarks and gluinos) production.

Recall that for mSUGRA Point A the signal is dominated by $H^0, A^0 \to \widetilde{\chi}_2^0\widetilde{\chi}_2^0$ decays, whereas for mSUGRA Point B heavier –inos make major contributions. Thus, a wedgebox plot analysis of the former is expected to show a simple box topology, while in the case of the latter there unfortunately may be too few events (even with $300\,\mathrm{fb}^{-1}$ of integrated luminosity) to clearly discern a pattern. For mSUGRA Point B, 9(10) signal events survive after all cuts (save the 4ℓ inv. m. cut), while 6 background events survive, assuming $100\,\mathrm{fb}^{-1}$ of integrated luminosity. This is insufficient to claim a discovery by the criterion of Relation (2). However, when the integrated luminosity is increased to $300\,\mathrm{fb}^{-1}$, then the raw number of signal events suffices to cross the discovery threshold. Unfortunately though, for mSUGRA Point B the background from colored sparticle production is not removed by the upper limit imposed on E_T^{jet}. One can however stiffen the E_T^{jet} cut, capping the allowable jet transverse energy at

30 GeV rather than 50 GeV and thus eliminate much of this background without diminishing the signal rate significantly. Then, with 300 fb^{-1} of integrated luminosity the discovery criteria can be met.

An earlier ATLAS study [47, 16] also sought to map out the discovery reach of the Higgs boson to neutralino four-lepton signature within the mSUGRA framework transposed onto the (M_A, $\tan\beta$) plane. Though some statements to the contrary are included in this ATLAS study, it does seem to have been focused on the $\widetilde{\chi}_2^0\widetilde{\chi}_2^0$ contributions (analogous to previously-discussed general MSSM studies of this signature), thus apparently omitting parameter sets such as mSUGRA Point B considered herein. Thus, the viability of mSUGRA Point B indicates an enlargement of the signal discovery region to higher values of M_A (and the mSUGRA parameter M_0) at intermediate values of $\tan\beta$ (*i.e.*,in the 'decoupling' region) from that reported in this ATLAS study (akin to the enlargements shown in the general MSSM case, though the extent of this enlargement in the case of mSUGRA models will not be quantified herein).

Table 5: Event rates after the successive cuts defined in the text for mSUGRA Point A (assuming an integrated luminosity of 100 fb^{-1}).

Process	4ℓ events	$\ell^+\ell^-\ell^{(\prime)+}\ell^{(\prime)-}$	Z^0-veto	E_T^{ℓ}	E_T^{miss}	E_T^{jet}	4ℓ inv. m.
$\widetilde{q}$, $\widetilde{g}$	927	504	312	280	174	0	0
$\widetilde{\ell}$,$\widetilde{\nu}$	326	178	145	117	100	71	58
$\widetilde{\chi}\widetilde{\chi}, \widetilde{q}/\widetilde{g}\widetilde{\chi}$	567	294	203	179	121	29	21
tH^- + c.c.	1	0	0	0	0	0	0
$Z^{0(*)}Z^{0(*)}$	1733	1683	43	39	5	4	4
$t\bar{t}Z^{0(*)}$	47	23	2	1	1	0	0
$t\bar{t}h^0$	4	2	2	1	1	0	0
H^0, A^0 signal	46,140	40,123	38,122	38,120	30,83	24,66	24,66

Table 6: Event rates after the successive cuts defined in the text for mSUGRA Point B (assuming an integrated luminosity of 100 fb^{-1}).

Process	4ℓ events	$\ell^+\ell^-\ell^{(\prime)+}\ell^{(\prime)-}$	Z^0-veto	E_T^{ℓ}	E_T^{miss}	E_T^{jet}	4ℓ inv. m.
$\widetilde{q}$, $\widetilde{g}$	4504	2598	1911	1672	917	12	12
$\widetilde{\ell}$,$\widetilde{\nu}$	309	169	134	110	94	67	57
$\widetilde{\chi}\widetilde{\chi}, \widetilde{q}/\widetilde{g}\widetilde{\chi}$	579	302	206	174	115	32	27
tH^- + c.c.	1	1	0	0	0	0	0
$Z^{0(*)}Z^{0(*)}$	1733	1683	43	39	5	4	4
$t\bar{t}Z^{0(*)}$	47	23	2	1	1	0	0
$t\bar{t}h^0$	5	2	1	1	1	0	0
H^0, A^0 signal	43,130	38,118	37,116	37,116	29,93	23,75	23,75

5 Wedgebox analysis of Higgs boson decays to –ino pairs

The wedgebox plot technique was introduced in a previous work [27] which focused on neutralino pairs produced via colored sparticle production and subsequent 'cascade' decays. Another work [48] has just recently focused on neutralino pairs produced via EW processes, including via a $Z^{0(*)}$ boson or via H^0,A^0 production; the former is termed 'direct' production while the latter is 'Higgs-mediated' production. A jet cut was found to be fairly efficient in separating these two neutralino pair-production modes from cascade production assuming the colored gluinos and squarks are fairly heavy.

To utilize the wedgebox technique, the criteria for the final four-lepton state are further sharpened by demanding that the final state consist of one e^+e^- pair and one $\mu^+\mu^-$ pair [26]. The wedgebox plot then consists of the $M(\mu^+\mu^-)$ invariant mass plotted versus the $M(e^+e^-)$ invariant mass for all candidate events. If a given neutralino, $\widetilde{\chi}_i^0$, decays to the LSP, $\widetilde{\chi}_1^0$, and a charged lepton pair via a three-body decay mediated by a virtual Z^{0*} or virtual/off-mass-shell charged slepton, then $M(\ell^+\ell^-)$ is bounded from above by $m_{\widetilde{\chi}_i^0} - m_{\widetilde{\chi}_1^0}$ (and from below by 0 if lepton masses are neglected). Given a sufficient number of events, the wedgebox plot of the signal events will be composed of a superposition of 'boxes' and 'wedges' [27], in the $M(e^+e^-)$-$M(\mu^+\mu^-)$ plane resulting from decay chains of the form:

$$H^0, A^0 \to \widetilde{\chi}_i^0 \widetilde{\chi}_j^0 \to e^+e^-\mu^+\mu^-\widetilde{\chi}_1^0\widetilde{\chi}_1^0 \; . \tag{3}$$

If $\widetilde{\chi}_i^0$ ($\widetilde{\chi}_j^0$) decays into an e^+e^- ($\mu^+\mu^-$) pair, then $M(e^+e^-)$ ($M(\mu^+\mu^-)$) is bounded above by $m_{\widetilde{\chi}_i^0} - m_{\widetilde{\chi}_1^0}$ ($m_{\widetilde{\chi}_j^0} - m_{\widetilde{\chi}_1^0}$). On the other hand, if $\widetilde{\chi}_i^0$ ($\widetilde{\chi}_j^0$) decays into a $\mu^+\mu^-$ (e^+e^-) pair, then these $M(e^+e^-)$ and $M(\mu^+\mu^-)$ upper bounds are swapped. Superposition of these two possibilities yields a 'box' when $i = j$ (which will be called an 'i-i box') and a 'wedge' (or 'L-shape') when $i \neq j$ (this will be called an 'i-j-wedge').

A heavy neutralino, $\widetilde{\chi}_i^0$, could instead decay to the $\widetilde{\chi}_1^0$ + leptons final state via a pair of two-body decays featuring an on-mass-shell charged slepton of mass[27] $m_{\widetilde{\ell}}$. Events containing such decays will lead to the same wedgebox pattern topologies as noted above; however, the upper bound on $M(\ell^+\ell^-)$ is modified to [50]

$$M(\ell^+\ell^-) < m_{\widetilde{\chi}_i^0}\sqrt{1-\left(\frac{m_{\widetilde{\ell}}}{m_{\widetilde{\chi}_i^0}}\right)^2}\sqrt{1-\left(\frac{m_{\widetilde{\chi}_1^0}}{m_{\widetilde{\ell}}}\right)^2} \; . \tag{4}$$

The $M(\ell^+\ell^-)$ spectrum is basically triangular in this case and sharply peaked toward the upper bound, while the former three-body decays yield a similar but less sharply peaked spectrum. The two-body decay series alternatively could be via an on-mass-shell Z^0, resulting in an $M(\ell^+\ell^-) = M_Z$ spike.

Additional complications can arise if the heavy neutralino $\widetilde{\chi}_i^0$ can decay into another neutralino $\widetilde{\chi}_j^0$ ($j \neq 1$) or a chargino which subsequently decays to yield the $\widetilde{\chi}_1^0$ final state. These

[26] In fact, this extra restriction is not strictly necessary, since recent preliminary work shows same-flavor four-lepton final states can be correctly paired with a reasonably high efficiency for at least some processes and some points in the MSSM parameter space [49].

[27] Note that this is the physical slepton mass, not the soft mass input.

may introduce new features to the wedgebox plot: $\widetilde{\chi}_i^0$ to $\widetilde{\chi}_j^0$ ($j \neq 1$) decay chains involving $\widetilde{\chi}_3^0 \to \ell^+\ell^-\widetilde{\chi}_2^0$, $\widetilde{\chi}_4^0 \to \ell^+\ell^-\widetilde{\chi}_2^0$, and/or $\widetilde{\chi}_4^0 \to \ell^+\ell^-\widetilde{\chi}_3^0$ will generate additional abrupt event population changes or edges, termed 'stripes,' on the wedgebox plot. One can imagine quite elaborate decay chains, with $\widetilde{\chi}_4^0 \to \widetilde{\chi}_3^0 \to \widetilde{\chi}_2^0 \to \widetilde{\chi}_1^0$ for instance. However, such elaborate chains are very unlikely to emerge from any reasonable or even allowed choice of MSSM input parameters. Further, each step in such elaborate decay chains either produces extra visible particles in the final state or one must pay the price of the BR to neutrino-containing states. The latter tends to make the contribution from such channels insignificant, while the former, in addition to also being suppressed by the additional BRs, may also be cut if extra restrictions are placed on the final state composition in addition to demanding an e^+e^- pair and a $\mu^+\mu^-$ pair. The aforementioned extra visible particles could be two more leptons, meaning that all four leptons come from only one of the initial -inos, $\widetilde{\chi}_i^0 \to \ell^+\ell^-\widetilde{\chi}_k^0 \to \ell^+\ell^-\ell'^+\ell'^-\widetilde{\chi}_1^0$, while the other –ino, which must yield no leptons (or other visible final state SM particles forbidden by additional cuts), decays via $\widetilde{\chi}_j^0 \to \nu\bar{\nu}\widetilde{\chi}_1^0$ or $\widetilde{\chi}_j^0 \to q\bar{q}\widetilde{\chi}_1^0$. Again though such channels will be suppressed by the additional required BRs. A further caveat is that decays with extra missing energy (carried off by neutrinos, for example) or missed particles can further smear the endpoint. The presence of charginos may also further complicate the wedgebox picture. Heavier –inos can decay to the LSP + lepton pair final state via a chargino, $\widetilde{\chi}_i^0 \to \ell^+\nu\widetilde{\chi}_1^- \to \ell^+\nu\ell'^-\bar{\nu}'\widetilde{\chi}_1^0$, or a Higgs boson itself may decay into a chargino pair, with one chargino subsequently yielding three leptons while the other chargino yields the remaining one (such events are called '3+1 events' [48]). The chargino yielding three leptons will typically decay via a $\widetilde{\chi}_2^0$, resulting in a re-enforcement of the solely –ino-generated wedgebox plot topology. A single chargino-generated lepton paired with another lepton from a different source produces a wedge-like structure but with no definite upper bound. For a more in-depth discussion of these nuances, see [48].

The right-hand plot in Fig. 9 shows the wedgebox plot obtained in the case of MSSM Point 1, assuming an integrated LHC luminosity of $300\,\text{fb}^{-1}$. Criteria for event selection are as given in the previous section, save that the more restrictive demand of an $e^+e^-\mu^+\mu^-$ final state is applied while the Z^0-veto and four-lepton invariant mass cuts are not applied. Both signal and background events are included; the former are colored black. The latter consist of both SM backgrounds (on- or off-mass-shell Z^0-boson pair-production — $Z^{0(*)}Z^{0(*)}$, 83 events, and $t\bar{t}Z^{0(*)}$, largely removed by the missing energy and jet cuts, 2 remaining events; these events are colored red and purple, respectively, in Fig. 9) and MSSM sparticle production processes ('direct' neutralino or chargino production, 4 events, and slepton pair-production, 22 events; such events are colored green and blue, respectively, in Fig. 9). No events from colored sparticle production survive the cuts, particularly the jet cut — this is a crucial result. Signal events consist of 14 H^0 events and 25 A^0 events, yielding a signal to background of $39 : 111 = 1 : 2.85$. With $S/\sqrt{B} = 3.7$, this is not good enough to claim a discovery based on Relation (2). If the input CP-odd Higgs boson mass is lowered to $M_A = 400\,\text{GeV}$, whose wedgebox plot is the left-hand plot of Fig. 9, then the number of signal events rises to $14 + 52 = 66$ H^0 and A^0 events (runs for MSSM backgrounds gave 2 'direct' neutralino-chargino events and 26 slepton-pair production events), yielding $S/\sqrt{B} = 6.2$ and satisfying Relation (2). Note how the increase is solely due to more A^0-generated events. Comparing the $M_A = 500\,\text{GeV}$ (MSSM Point 1) plot (b) and the $M_A = 400\,\text{GeV}$ plot (a) in Fig. 9 shows how the increased number of signal events in (a) more fully fills in the 2-2 box whose outer edges (dashed lines in the figure) are

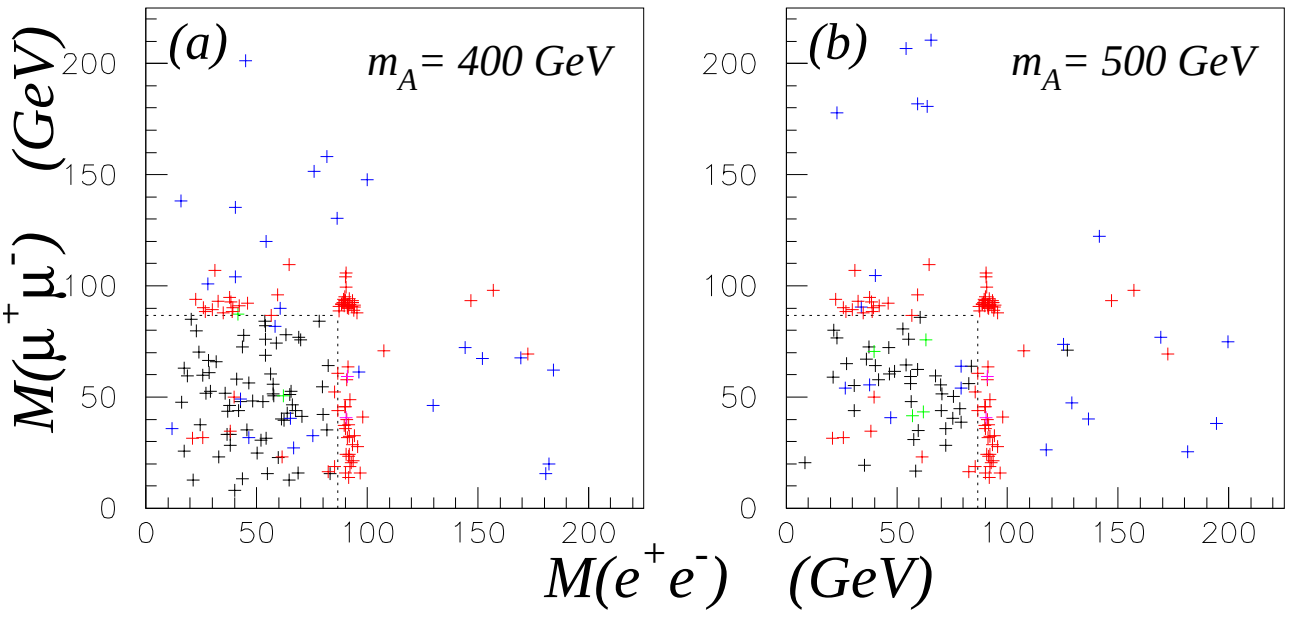

Figure 9: Wedgebox plot for MSSM Point 1 inputs with $M_A = 500\,\text{GeV}$ (b) and shifting to $M_A = 400\,\text{GeV}$ (a), assuming an integrated luminosity of $300\,\text{fb}^{-1}$. Neither the Z^0-veto cut nor the 4-lepton invariant mass cut are enabled. Black-colored markers are for the H^0 and A^0 signal events. SM background events from $Z^{0(*)}Z^{0(*)}$ (where either one or both of the Z^0's are permitted to be off-mass-shell are red), while the two surviving $t\bar{t}Z^{0(*)}$ events are purple. MSSM background events from slepton production or direct neutralino/chargino production are in blue and green, respectively. The horizontal and vertical dashed lines forming a box are at the location $m_{\widetilde{\chi}_2^0} - m_{\widetilde{\chi}_1^0}$. MSSM Point 1 –ino and slepton inputs are $\mu = -500\,\text{GeV}$, $M_2 = 180\,\text{GeV}$, $M_1 = 90\,\text{GeV}$, $m_{\widetilde{\ell}_{soft}} = m_{\widetilde{\tau}_{soft}} = 250\,\text{GeV}$.

given by $m_{\widetilde{\chi}_2^0} - m_{\widetilde{\chi}_1^0} = 86.6\,\text{GeV}$ since for these input parameters slepton masses are too high to permit $\widetilde{\chi}_2^0$ decays into on-mass-shell sleptons.

A key observation is that the distributions of the signal and the background events differ markedly[28]. All but one of the signal events lie within the 2-2 box[29]. The majority of the slepton pair-production events (19 out of 26 events for (a) and 17 out of 22 events for (b)), the dominant MSSM background, lie outside the 2-2 box. The topology of these '3+1' events is a 2-2 box plus a wedge lacking a clear outer edge extending from said box (see [48]). The few 'direct' neutralino and chargino production events happen to all lie within the 2-2 box; however, these events are actually due to[30] $\widetilde{\chi}_2\widetilde{\chi}_3$ pair-production and thus, for a larger sample,

[28]On the other hand, the distributions of A^0 and H^0 events show no substantial systematic differences in their distributions' wedgebox plot topologies.

[29]Note that a similar result is found in Fig. 16 of [9]. There, however, only signal events were shown, and, since *a priori* only $H^0, A^0 \to \widetilde{\chi}_2^0\widetilde{\chi}_2^0$ events were considered, the vast array of other potential wedgebox topologies was not brought to light.

[30]If direct neutralino pair-production produces a significant number of events, then the dominant source of said events is always $\widetilde{\chi}_2^0\widetilde{\chi}_3^0$ production; $\widetilde{\chi}_2^0\widetilde{\chi}_2^0$ production is heavily suppressed. See discussion in [48]. This

such events would populate a 2-3 wedge with many of the events falling outside of the 2-2 box.

SM background events are concentrated on and around lines where either $M(e^+e^-)$ and/or $M(\mu^+\mu^-)$ equals M_Z, which unfortunately is close to the outer edges of the 2-2 box. Using the unfair advantage of color-coded events, one can correctly choose to place the edges of the box so as to exclude most of the SM background events. Experimentalists may have a more difficult time deciding on wedgebox edges that lie too close to M_Z. Though, at the price of perhaps losing some of the signal events[31], one could make a selection rule of an effective 2-2 box with edges sufficiently within M_Z in such cases. Correct identification of the outer edge value for the 2-2 box removes all but 11 of the 85 SM background events. The signal:background is then 39 : 20 for (b) and 66 : 19 for (a), an immense improvement in the purity of the samples — both points now certainly satisfy the Relation (2) criterion. Accepting only points lying within a box with outer edges at 80 GeV, more safely eliminating SM $Z^{0(*)}Z^{0(*)}$ events, leads to a signal:background of 33 : 12 for (b) and 59 : 14 for (a). Note that one can also select points lying well outside the 2-2 box to get a fairly pure sample (at this point in the parameter space) of slepton pair-production events. Even if one does not know where Nature has chosen to reside in the MSSM input parameter space, the selection of only events occupying one distinct topological feature of the experimental wedgebox plot may yield a sample pure enough (though one may not know exactly what purified sample one has obtained!) to be amenable to other means of analysis (perhaps entailing some addition reasonable hypotheses as to what sparticles might be involved) [51].

Fig. 10 in turn examines several related choices for input parameter sets, including MSSM Point 2 — which is plot (c) therein, in which H^0 and A^0 have large BRs into heavier –ino pairs such that the majority of the 4ℓ signal events do not arise from $\widetilde{\chi}_2^0\widetilde{\chi}_2^0$ decays for all points save that of plot (b). Plot (d) differs from MSSM Point 2, plot (c), only in that the Higgsino mixing parameter μ is shifted from $\mu = -200\,\mathrm{GeV}$ to $\mu = -250\,\mathrm{GeV}$. Yet even this modest change drastically alters the topology of the resulting wedgebox plot. This is illustrative of how the wedgebox plot may be useful in extracting fairly detailed information about the –ino spectrum and corresponding MSSM input parameters. In plots (a) and (b) of Fig. 10 the EW gaugino input parameters are raised from $M_2 = 200\,\mathrm{GeV}$ in plots (c) and (d) to $M_2 = 280\,\mathrm{GeV}$ (recall the assumption used herein that the value of M_1 is tied to that of M_2). Also $\tan\beta$ is lowered from 35 to 20, while μ values of plots (c) and (d) are retained. Again, these shifts in input parameters radically alter the resulting wedgebox topology. Plots (a) and (b) clearly show wedge-like topologies. Note again the markedly different event distributions for the signal and background events in all four plots, but particularly striking in plot (a). Note how the four MSSM parameter set points yielding the wedgebox plots depicted in Fig. 10 all might crudely be categorized as high $\tan\beta$, low $|\mu|$, low to moderate M_2, and light slepton points. Yet the associated wedgebox plots come out decidedly different.

Taking advantage of knowing which points in MSSM parameter space are being simulated

leads to the general conclusion that, with a jet cut in place to remove cascade events from colored sparticle decays, the appearance of a disproportionately strong (densely populated) box on a wedgebox plot is highly indicative of the presence of Higgs-boson-generated events. The caveat to this being that chargino production can generate a box-shape in some rather limited regions of the MSSM input parameter space. Again, see [48] for further discussion.

[31] Correct edge values from which to reconstruct information on the –ino mass spectrum would also be lost.

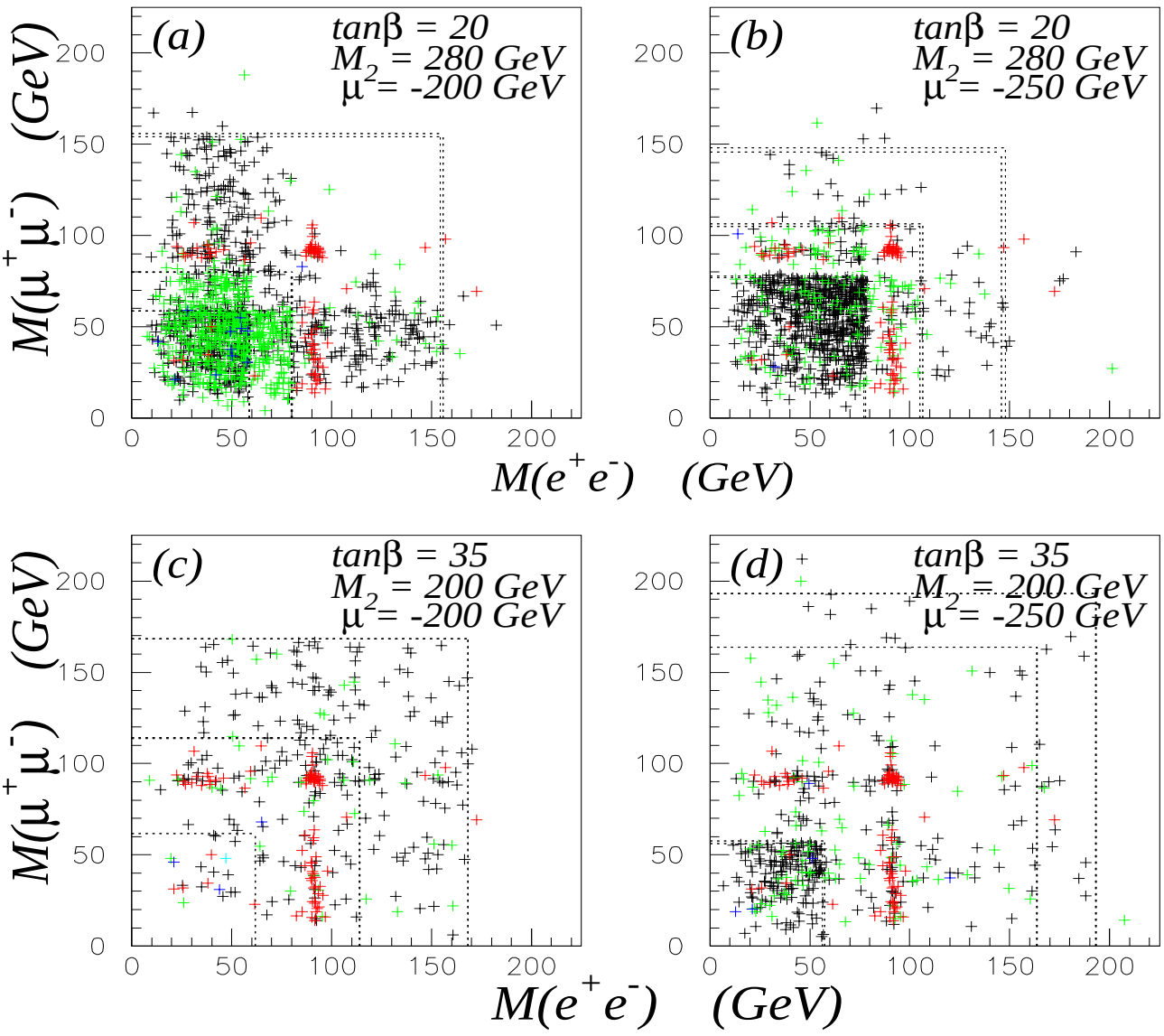

Figure 10: Wedgebox plot for MSSM Point 2 inputs (c) and shifting to $M_A = 400\,\text{GeV}$ (left), assuming an integrated luminosity of $300\,\text{fb}^{-1}$. Neither the Z^0-veto cut nor the 4-lepton invariant mass cut are enabled. Black-colored markers are for the H^0 and A^0 signal events. SM background events from $Z^{0(*)}Z^{0(*)}$ (where either one or both of the Z^0's are permitted to be off-mass-shell) are red, while the two surviving $t\bar{t}Z^{0(*)}$ events are purple. MSSM background events from slepton production or direct neutralino/chargino production are in blue and green, respectively. The horizontal and vertical dashed lines forming a box are at the location $M_{\widetilde{\chi}_2^0} - M_{\widetilde{\chi}_1^0}$. MSSM Point 1 –ino and slepton inputs are $\mu = -500\,\text{GeV}$, $M_2 = 180\,\text{GeV}$, $M_1 = 90\,\text{GeV}$, $m_{\widetilde{\ell}_{soft}} = m_{\widetilde{\tau}_{soft}} = 250\,\text{GeV}$. Also indicated by dashed lines on the plot are the 2-2, 3-3 and 4-4 box edges found from relation (4) — save for the 2-2 box edges for (c) which are from $m_{\widetilde{\chi}_2^0} - m_{\widetilde{\chi}_1^0}$.

Table 7: Percentage contributions to $H^0, A^0 \to 4\ell$ events from the various neutralino and chargino pair-production modes for the four MSSM Parameter set points given in Fig. 10. Based upon ISAJET(ISASUSY) 7.58 [30] with no consideration given to any cuts. Decays that are kinematically not allowed are marked by a 0; contributions below 0.001% are marked as negligible (*neg*). $H^0, A^0 \to Z^{0(*)}Z^{0(*)}$, $H^0 \to h^0h^0$ and $A^0 \to h^0Z^{0(*)}$ make negligible contributions in all cases. Also given are the number of H^0,A^0 signal events and the number of background events, assuming $300\,\mathrm{fb}^{-1}$ of integrated luminosity as in the figure.

Decay Pair	(a)	(b)	(c)	(d)
$\widetilde{\chi}_2^0\ \widetilde{\chi}_2^0$	18.6%	70.6%	0.0015%	35.0%
$\widetilde{\chi}_2^0\ \widetilde{\chi}_3^0$	0.1%	4.5%	0.05%	13.1%
$\widetilde{\chi}_2^0\ \widetilde{\chi}_4^0$	45.1%	13.0%	0.05%	1.6%
$\widetilde{\chi}_3^0\ \widetilde{\chi}_3^0$	1.5%	0.4%	2.7%	0.9%
$\widetilde{\chi}_3^0\ \widetilde{\chi}_4^0$	18.1%	5.0%	45.0%	9.5%
$\widetilde{\chi}_4^0\ \widetilde{\chi}_4^0$	0	0	39.6%	7.8%
$\widetilde{\chi}_1^\pm\ \widetilde{\chi}_2^\mp$	16.6%	6.5%	11.3%	31.8%
$\widetilde{\chi}_2^+\ \widetilde{\chi}_2^-$	0	0	1.4%	0.3%
$\widetilde{\chi}_1^0\ \widetilde{\chi}_3^0$	0.001%	0.005%	*neg*	0.05%
$\widetilde{\chi}_1^0\ \widetilde{\chi}_4^0$	0.02%	*neg*	*neg*	0.01%
H^0, A^0 evts.	305,423	276,473	122,105	182,140
bckgrd. evts.	683	257	132	186

(something the experimentalist cannot know in the actual experiment) allows comparison between the assorted calculated production rates at the four points and the observed features on the wedgebox plots. Table 7 gives such theoretical estimates based on analysis of ISAJET (ISASUSY) 7.58 results for the four points[32]. It must be borne in mind though that effects from cuts may alter the percentage contributions found on the wedgebox plots from those given in Table 7.

The first thing to notice from this table is the virtual absence of events stemming from $\widetilde{\chi}_2^0$ to $\widetilde{\chi}_1^0$ decays for MSSM Point 2 = plot (c) relative to the other three points. This is due to the fact that, for this input parameter set, the sparticle spectrum satisfies the condition that $m_{\widetilde{\nu}} < m_{\widetilde{\chi}_2^0} < m_{\widetilde{\ell}^\pm}$, meaning that $\widetilde{\chi}_2^0$ mainly decays via an on-mass-shell sneutrino 'spoiler' mode, $\widetilde{\chi}_2^0 \to \widetilde{\nu}\bar{\nu} \to \widetilde{\chi}_1^0\nu\bar{\nu}$, and its BR into a pair of charged leptons is highly suppressed. For the other three points, $m_{\widetilde{\chi}_2^0} > m_{\widetilde{\ell}^\pm}, m_{\widetilde{\nu}}$. Actually, of the four wedgebox plots shown in Fig. 10, the one for MSSM Point 2 most closely resembles a simple box. However, Table 7 indicates that (before cuts) 45.0% of the events are from $\widetilde{\chi}_3^0\widetilde{\chi}_4^0$, 39.6% of the events are from $\widetilde{\chi}_4^0\widetilde{\chi}_4^0$, and 12.7% of the events are from $\widetilde{\chi}_1^\pm\widetilde{\chi}_2^\mp$, $\widetilde{\chi}_2^+\widetilde{\chi}_2^-$.

In Fig. 10, charged sleptons are now light enough so that the neutralino to slepton decay chains, which make significant contributions to the four-lepton signal events, may proceed via on-mass-shell charged sleptons. So while the outer edges of the 2-2 box in Fig. 9 was

[32]Table 3 given previously corresponds to column (c) in Table 7 with the H^0 and A^0 contributions listed separately.

determined by the $\widetilde{\chi}_2^0$-$\widetilde{\chi}_1^0$ mass difference, here Relation 4 brings the slepton masses into play[33]. In plot (a), virtually all $\widetilde{\chi}_i^0$ to $\widetilde{\chi}_1^0$ decays proceed via on-mass-shell sleptons, but only the $\widetilde{\chi}_4^0$ to $\widetilde{\chi}_1^0$ decay edge is significantly altered (by more than a couple GeV) — from $m_{\widetilde{\chi}_4^0} - m_{\widetilde{\chi}_4^0} = 185\,\text{GeV}$ to 151-156 GeV (at this point, 18% of four-lepton events are from $\widetilde{\chi}_3^0\widetilde{\chi}_4^0$ according to Table 7). On the other hand, in plot (b), where the $\widetilde{\chi}_i^0$ also decay to $\widetilde{\chi}_1^0$ via on-mass-shell sleptons, edges are shifted from $m_{\widetilde{\chi}_i^0} - m_{\widetilde{\chi}_1^0} = 82, 124, 192\,\text{GeV}$ to 76-78, 101-107, 140-149 GeV for $i = 2, 3, 4$, respectively[34], with $i = 2, 3, 4$ decays all making noteworthy four-lepton event contributions. For MSSM Point 2 = plot (c), the shift in the $\widetilde{\chi}_3^0$ to $\widetilde{\chi}_1^0$ decay edge is only 3.5-5 GeV while the $\widetilde{\chi}_4^0$ to $\widetilde{\chi}_1^0$ edge is virtually unchanged. This accounts for 87.3% of the four-lepton events by Table 7. The situation with $\widetilde{\chi}_2^0$ is slightly complicated: $\widetilde{\chi}_2^0$ can only decay into $\widetilde{\chi}_1^0$ via an on-mass-shell[35] $\widetilde{\mu}_1$, and this would lead to a tremendous shift in the edge position (from 61 GeV to 15 GeV); however, this is so close to the kinematical limit that decays through off-mass-shell Z^{0*} should be competitive (again placing the edge at ∼61 GeV). *But*, since $\widetilde{\chi}_2^0$ decays lead to only a tiny fraction of the four-lepton events, note how there is no visible edge or population discontinuity at this location (the innermost dashed box) on the wedgebox plot. Lastly, with plot (d), again on-mass-shell slepton decays totally dominate for $i = 2, 3, 4$, but only the $\widetilde{\chi}_2^0$ to $\widetilde{\chi}_1^0$ decay edge is significantly shifted (from 75.2 GeV to 51.5-60.4 GeV[36]. But, by Table 7, this decay is the most important contributor to the signal events.

For plot (a) of Fig. 10, the expected 2-4 wedge stands out clearly among the signal events, with outer edges at the expected location. The background is mostly from direct $\widetilde{\chi}_2^0\widetilde{\chi}_3^0$ direct production, giving the 2-3 wedge shown in green (direct neutralino-neutralino production is predominantly $\widetilde{\chi}_2^0\widetilde{\chi}_3^0$ at all interesting points in the MSSM parameter space, with direct $\widetilde{\chi}_2^0\widetilde{\chi}_2^0$ production always highly suppressed [48]). The proximity of this wedge's outer edges to the red M_Z lines may complicate the experimental analysis; however, if the SM $Z^{0(*)}Z^{0(*)}$ background is well-modeled, a subtraction technique to clear up this zone may be feasible. Note that selecting only events with $100\,\text{GeV} < M(e^+e^-) < 150\,\text{GeV}$, $0 < M(\mu^+\mu^-) < 50\,\text{GeV}$ or $0 < M(e^+e^-) < 50\,\text{GeV}$ $100\,\text{GeV} < M(\mu^+\mu^-) < 150\,\text{GeV}$, corresponding to the legs of the 2-4 wedge lying beyond the 2-3 wedge and the Z^0-line, changes the signal:background ratio from 728:683 seen on the plot to 128:15. This is an example of a cut that can be applied *a posteriori* based on the examination of the wedgebox plot — as opposed to assuming *a priori* extra knowledge about where in the MSSM parameter space Nature has chosen to sit.

Plot (b) of Fig. 10 mainly shows a densely-populated 2-2 box whose edges are well inside the M_Z lines. A faint 2-3 or 2-4 wedge is also discernible (in fact Table 7 shows this to be a

[33]Unfortunately, the physical slepton masses input into HERWIG 6.5 are generated by ISASUSY 7.58 [30], which neglects a left-right mixing term $\propto m_\ell^2\mu^2\tan^2\beta$ (see [27]). While this term is negligible for selectrons, it does shift the physical smuon masses by as much as a few GeV. Neglecting this term results in degenerate soft slepton inputs leading to degenerate physical selectron and smuons masses (so the smuon masses for MSSM Point 2 given in Table 1 are changed into the mass values given there for the selectrons), which in turn may noticeably under-estimate the mass splitting between smuons and thus the thickness of the edges shown on the plots. Later versions of ISAJET correct this oversight, as do private codes employed in Sect. 2.

[34]Due to the program oversight mentioned in the last footnote, the thicknesses of these edges shrink to 75.7-76.5, 103.4-104.9, 143.5-145.9 GeV, respectively. These values are represented by the dotted lines on the plots.

[35]Again, this feature is lost in HERWIG 6.5/ISAJET 7.58 .

[36]In HERWIG 6.5/ISAJET 7.58 this width shrinks to 55.6-57.0 GeV.

2-4 wedge), while the empty upper-right corner which does not join with the 2-2 box suggests that $\widetilde{\chi}_2^0\widetilde{\chi}_4^0$ and $\widetilde{\chi}_3^0\widetilde{\chi}_4^0$ decays are present while $\widetilde{\chi}_4^0\widetilde{\chi}_4^0$ are absent (further suggesting that said decay mode is kinematically inaccessible, which helps pin down the relative masses of the heavy Higgs bosons and the heavier neutralinos).

Plot (c)'s most obvious feature is an outer box, which in fact is a 4-4 box. Topology alone does not distinguish this from a plot dominated by a 3-3 box or a 2-2 box, though the location of the outer edges well beyond M_Z might give pause for entertaining the latter possibility. A 3-4 wedge may also be discerned from the somewhat diminished event population in the upper right-hand box in the plot. Comparison of this plot with the other three quickly points out the absence of a dense event-population in this plot. Seeing such a wedgebox plot experimentally strongly hints that leptonic $\widetilde{\chi}_2^0$ decays are being suppressed, perhaps with a mass spectrum favoring sneutrino spoiler modes as noted above.

Like plot (b), plot (d) shows a 2-2 box, but with outer edges at a very different location. Plot (d) also has more signal events outside of the 2-2 box than does plot (b), and said events are more scattered in (d). A lot of these events are from H^0, A^0 decays into $\widetilde{\chi}_1^\pm\widetilde{\chi}_2^\mp$ pairs. Thus, the alignment of the wedgebox features to the dashed lines derived from neutralino features shown is less compelling.

In both Fig. 9 and Fig. 10, note how closely the wedgebox plot features, obtained by the full event generator & detector simulation analysis, conform to the dashed-line borders expected from the simple formula 4. This strongly supports the assertion that a wedgebox-style analysis is realistic in the actual experimental situation.

6 Summary and conclusions

Recapping the findings presented herein:

6.1 New signals

For many interesting choices of the basic input parameters of the MSSM, heavier Higgs boson decay modes of the type $H^0, A^0 \to \widetilde{\chi}_i^0\widetilde{\chi}_j^0$, with $i, j \neq 1$ are potentially important LHC signal modes. The neutralinos' subsequent leptonic decays, typified by $\widetilde{\chi}_i^0 \to \ell^+\ell^-\widetilde{\chi}_1^0$, can yield a four-isolated-lepton (where here ℓ refers to electrons and/or muons) plus missing-transverse-energy signature. Such leptonic neutralino decays may proceed via either an intermediate charged slepton or via an intermediate $Z^{0(*)}$, where in either case this intermediate state may be on- or off-mass-shell. The present study presents for the first time a systematic investigation of the potential for discovering such a signature at the LHC, including all possible such neutralino pairs: $\widetilde{\chi}_2^0\widetilde{\chi}_2^0, \widetilde{\chi}_2^0\widetilde{\chi}_3^0, \widetilde{\chi}_2^0\widetilde{\chi}_4^0, \widetilde{\chi}_3^0\widetilde{\chi}_3^0, \widetilde{\chi}_3^0\widetilde{\chi}_4^0$, and $\widetilde{\chi}_4^0\widetilde{\chi}_4^0$. Other Higgs boson decays that may lead to the same signature are also incorporated, including: decays to chargino pairs $H^0, A^0 \to \widetilde{\chi}_1^\pm\widetilde{\chi}_2^\mp, \widetilde{\chi}_2^+\widetilde{\chi}_2^-$, in which case $\widetilde{\chi}_2^\mp$ yields three leptons while the other chargino gives the fourth; $H^0, A^0 \to \widetilde{\chi}_1^0\widetilde{\chi}_3^0, \widetilde{\chi}_1^0\widetilde{\chi}_4^0$, where the $\widetilde{\chi}_3^0$ or $\widetilde{\chi}_4^0$ must provide all four leptons; and $H^0 \to h^0h^0, Z^{0(*)}Z^{0(*)}$, $A^0 \to h^0Z^{0(*)}$, & $H^0, A^0 \to \widetilde{\ell}^+\widetilde{\ell}^-$, all three of which yield negligible contributions in all cases studied. This surpasses previous studies which restricted virtually all of their attention to $H^0, A^0 \to \widetilde{\chi}_2^0\widetilde{\chi}_2^0$, and also did not consider the possibility of neutralino

decays to on-mass-shell sleptons (with the incorporation of the heaviest neutralinos as is done herein this assumption becomes particularly restrictive).

Naturally, at least some of the –inos must be reasonably light for this $H^0, A^0 \to 4\ell + E_T^{\rm miss}$ signature to be seen. Parameter-space scans studying the potential scope of such a signal indicate that the –ino parameter M_2 needs to be relatively low while the Higgsino mixing parameter μ need not be so constrained (however, if $|\mu|$ is not also relatively low, then the signal is dominated by the $\widetilde{\chi}_2^0\widetilde{\chi}_2^0$ mode). Relatively light slepton masses are also quite helpful, and the slepton mass spectrum plays a crucial rôle in determining for what values of the other MSSM input parameters large rates may occur. Said large rates are possible throughout most of the phenomenologically-interesting value ranges of the Higgs-sector parameters M_A and $\tan\beta$, depending of course on the accompanying choice of other MSSM inputs, as the discovery regions delineated herein illustrate.

6.2 Comparison with previous results

To clearly demonstrate the potential importance of the $H^0, A^0 \to 4\ell + E_T^{\rm miss}$ signature in the hunt for the heavier Higgs bosons, Figs. 11 and 12 again show the discovery regions associated with MSSM Point 1 and MSSM Point 2 neutralino input parameter sets (as depicted before in Figs. 7 and 8, respectively), but this time with a logarithmic scale for $\tan\beta$ *and* also showing the expected reaches, assuming $300\,{\rm fb}^{-1}$ of integrated luminosity at the LHC, of Higgs boson decay modes into SM daughter particles as developed by the ATLAS collaboration [45][37]. Clearly, the new neutralino decay mode signature can extend the discovery reach for the heavier MSSM Higgs bosons to much higher values of M_A, and also offer at least partial coverage of the so-called 'decoupling region' where only the lightest Higgs state h^0 could be established in the past (through its decays into SM objects) and where said h^0 may be difficult to distinguish from the sole Higgs boson of the minimal SM. Thus, a more complete analysis of the $H^0, A^0 \to \widetilde{\chi}_i^0\widetilde{\chi}_j^0$ modes as is presented here may be crucial to the establishment of an extended Higgs sector. The inclusion of the heavier neutralinos, $\widetilde{\chi}_3^0$ and $\widetilde{\chi}_4^0$, absent in previous studies, is essential in extending the reach of the $H^0, A^0 \to 4\ell + E_T^{\rm miss}$ signature up to the higher Higgs boson masses unattainable by the SM decay modes.

It should be noted that the ATLAS discovery contours presented in Figs. 11 and 12 are *not* obtained using the same choice of MSSM input parameters as are the $H^0, A^0 \to \widetilde{\chi}_i^0\widetilde{\chi}_j^0$ discovery regions developed in the present work. In fact, the ATLAS discovery regions used input choices designed to eliminate, or at least minimize, the Higgs boson decays into sparticles. Thus, the reach of the ATLAS discovery contours essentially represents the maximum expanse in the MSSM parameter space achievable through these Higgs boson decays to SM particles under the (unsubstantiated) assumption of a very heavy sparticle sector. Stated another way: were the ATLAS discovery regions to be generated for the same set of neutralino input parameters as the $H^0, A^0 \to \widetilde{\chi}_i^0\widetilde{\chi}_j^0$ discovery regions presented herein, the former may well *shrink* in size (and certainly *not increase*), further emphasizing the importance of thoroughly studying the $H^0, A^0 \to 4\ell + E_T^{\rm miss}$ signature. It would certainly be desirable to re-do the SM-like signature reaches of MSSM Higgs bosons in the presence of light sparticle spectra identical to those

[37] ATLAS collaboration discovery region contour lines in Figs. 11 and 12 have been remade to match as closely as possible those in the original plot.

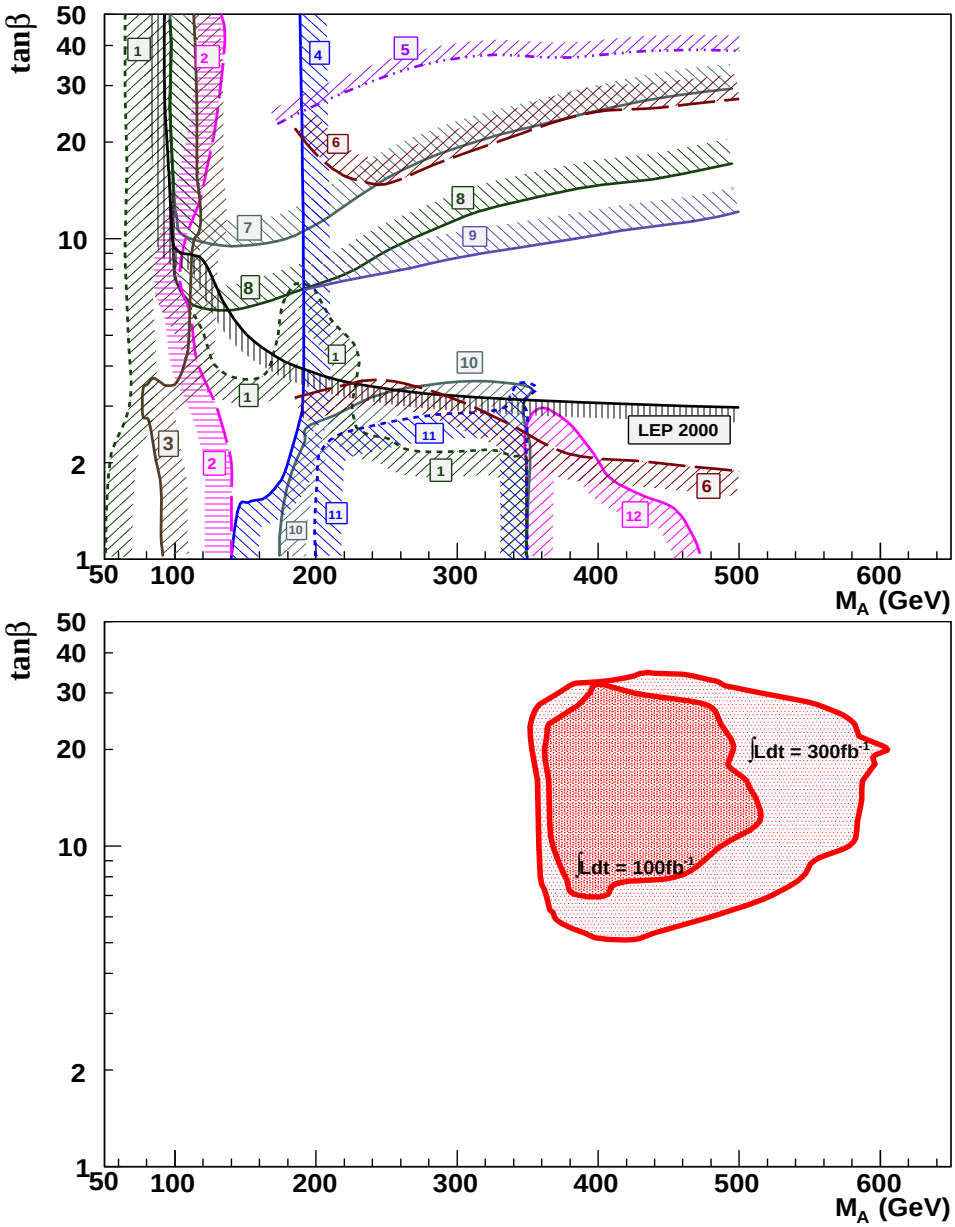

Figure 11: Discovery regions in the $(M_A, \tan\beta)$ plane, here with a logarithmic $\tan\beta$ scale, assuming MSSM Parameter Set 1 –ino inputs and for $\mathcal{L}_{int} = 100\,\text{fb}^{-1}$ and $300\,\text{fb}^{-1}$, for the (lower plot) MSSM Higgs bosons' 4ℓ signals from their decays into neutralino or chargino pairs (here H^0, A^0 decays to $\widetilde{\chi}^0_2\widetilde{\chi}^0_2$ totally dominate). This is shown juxtaposed (upper plot) with $300\,\text{fb}^{-1}$ regions for MSSM Higgs boson signatures from decays to SM particles based upon LEP results and ATLAS simulations [45], where labels represent: 1. $H^0 \to Z^0Z^{0*} \to 4\,\text{leptons}$; 2. $t \to bH^+$, $H^+ \to \tau^+\nu$ + c.c.; 3. $t\bar{t}h^0$, $h^0 \to b\bar{b}$; 4. $h^0 \to \gamma\gamma$ and $W^\pm h^0/tth^0$, $h^0 \to \gamma\gamma$; 5. $b\bar{b}H^0, b\bar{b}A^0$ with $H^0/A^0 \to b\bar{b}$; 6. $H^+ \to t\bar{b}$ + c.c.; 7. $H^0/A^0 \to \mu^+\mu^-$; 8. $H^0/A^0 \to \tau^+\tau^-$; 9. $g\bar{b} \to \bar{t}H+$, $H^+ \to \tau^+\nu$ + c.c.; 10. $H^0 \to h^0h^0 \to b\bar{b}\gamma\gamma$; 11. $A^0 \to Z^0h^0 \to \ell^+\ell^-b\bar{b}$; 12. $H^0/A^0 \to t\bar{t}$. Note that SM discovery regions are not for the same input parameters: they presume a very heavy sparticle spectrum; identical MSSM inputs to those used for the lower plot may well yield smaller SM discovery regions in a revised upper plot. For the 4ℓ signals from $\widetilde{\chi}^0_i\widetilde{\chi}^0_j, \widetilde{\chi}^+_m\widetilde{\chi}^-_n$ decays, the MSSM Parameter Set 1 –ino/slepton parameters are $\mu = -500\,\text{GeV}$, $M_2 = 180\,\text{GeV}$, $M_1 = 90\,\text{GeV}$ and $m_{\widetilde{\ell}_{soft}} = m_{\widetilde{\tau}_{soft}} = 250\,\text{GeV}$.

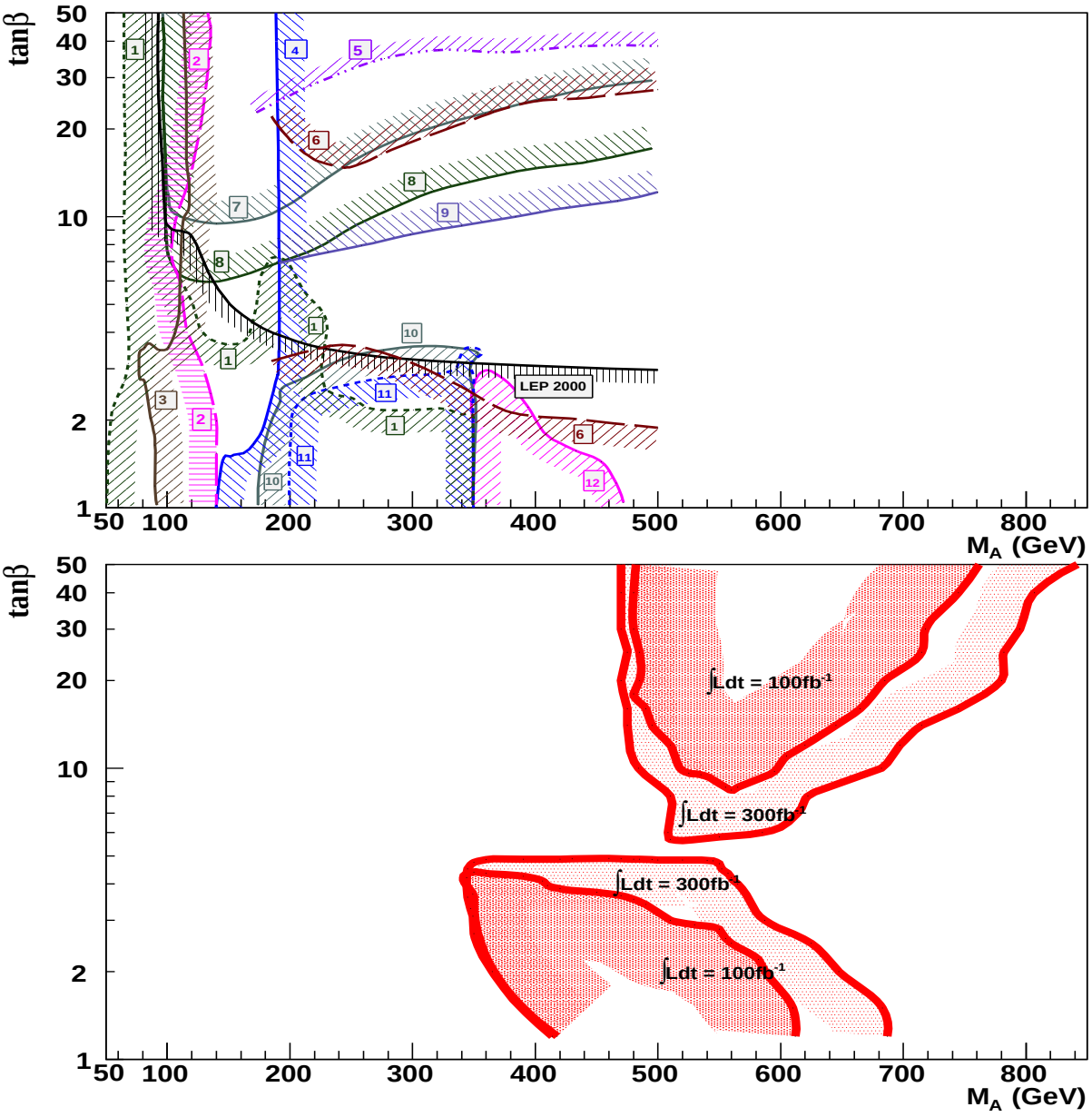

Figure 12: Discovery regions in the $(M_A, \tan\beta)$ plane, here with a logarithmic $\tan\beta$ scale, assuming MSSM Parameter Set 2 –ino inputs and for $\mathcal{L}_{int} = 100\,\text{fb}^{-1}$ and $300\,\text{fb}^{-1}$, for the (lower plot) MSSM Higgs bosons' 4ℓ signals from their decays into neutralino or chargino pairs (here Higgs boson decays to higher-mass neutralinos typically dominate). This is shown juxtaposed (upper plot) with $300\,\text{fb}^{-1}$ regions for MSSM Higgs boson signatures from decays to SM particles as in Fig. 11. For the 4ℓ signals from $\widetilde{\chi}_i^0\widetilde{\chi}_j^0$, $\widetilde{\chi}_m^+\widetilde{\chi}_n^-$ decays, the MSSM Parameter Set 2 –ino/slepton parameters are $\mu = -200\,\text{GeV}$, $M_2 = 200\,\text{GeV}$, $M_1 = 100\,\text{GeV}$, $m_{\widetilde{\ell}_{soft}} = 150\,\text{GeV}$ and $m_{\widetilde{\tau}_{soft}} = 250\,\text{GeV}$. Here Higgs boson decays to a variety of higher mass –inos (see text) constitute the majority of the signal events. Note that, as in Fig. 11, since ATLAS discovery regions presume a very heavy sparticle spectrum, SM discovery regions made for the same MSSM input parameters as used in the lower plot may well yield smaller SM discovery regions in a revised upper plot.

studied herein for the Higgs-to-sparticle decay channels; however, this is clearly beyond the scope and capabilities of this study. It also must be emphasized that the diminution of the expected signatures from SM decay modes of the MSSM Higgs bosons was investigated in [7] and thus is fairly well-established as well as inherently sensible.

Previous studies exploring Higgs-to-sparticle decay channels, whether for neutral Higgs bosons (*e.g.*, CMS [9]) or for charged Higgs bosons (*e.g.*, ATLAS [52], CMS [20]), — and comparing, to some extent, SM and SUSY decay modes — have not re-scaled the reaches of previously-studied SM decay channels (done by the same collaboration) to allow a reasonable comparison to the new-found sparticle decay modes; nor have the SM decay modes been re-analyzed for the same set of MSSM input parameters. Yet clearly such comparisons are absolutely essential to gauge the scope and impact of the new sparticle-decay channels. Certainly, the comparisons presented in Figs. 11 and 12 are less than optimal; however, they are far from un-informative.

It is also important to keep in mind that the assumptions inherent in the ATLAS (and CMS) discovery regions for the SM decay modes of the MSSM Higgs bosons are no less restrictive than the choices of MSSM input parameters made to generate the two $4\ell + E_T^{\rm miss}$ discovery regions in this study. The parameter space scans of Sect. 2 further enable the reader to put the two discovery regions shown here into a wider perspective.

6.3 Production and decay phenomenology of the signal

The new $H^0, A^0 \to 4\ell + E_T^{\rm miss}$ discovery regions have been mapped out using a full event generator-level analysis utilizing HERWIG coupled with a detector simulation on a par with experimental analyses. All significant backgrounds have been included in the analysis, some for the first time in the study of such a signature. The importance of the restriction on jet activity employed herein is particularly noteworthy. Without such a cut the Higgs signal could be swamped by the cascade decays of colored sparticles (gluinos and squarks), unless said sparticles are *a priori* assumed to be quite heavy (at or above the TeV scale). The ultimate limit of this type of jet cut, to demand that events be 'hadronically quiet' quickly springs to mind as an attractive search category. Yet care must be taken here since, in Higgs boson production via $gg \to H^0, A^0$ and $b\bar{b} \to H^0, A^0$, jets emerge in the final state alongside the Higgs bosons due to PS effects, though such additional jets tend to be rather soft and collinear to the beam directions. In addition, rather than emulating Higgs boson production via $gg \to H^0, A^0$ and $b\bar{b} \to H^0, A^0$, one could instead consider $gg \to ggH^0, ggA^0$ and $gg \to b\bar{b}H^0, b\bar{b}A^0$ processes, in which case one might worry about stronger jet activity emerging. The true signal rate is the sum of these and the previous process types, after making a correction for the overlap (as discussed previously). HERWIG simulations of $gg \to b\bar{b}H^0, b\bar{b}A^0$ at selected points in the parameter space indicate that the these processes are in fact removed by the jet cut imposed herein. To better optimize the level of hadronic activity that should be allowed, full implementation of $2 \to 3$ loop processes ($gg \to ggH^0, ggA^0$ and other channels yielding two light jets and a H^0, A^0 in the final state) into HERWIG must be completed (work in progress [53]).

The BRs of H^0 and A^0 to the assorted –ino pairs can certainly differ markedly in regions where the signal is large, as seen for instance in Table 3; thus one must not assume that the two contribute a roughly equal number of events to the $4\ell + E_T^{\rm miss}$ signal rate. On the

other hand, results also show that only in quite narrow low-M_A threshold regions within the discovery areas (wherein the small M_H-M_A mass difference is crucial) do events due to one or the other Higgs boson (in this case the lighter A^0) totally dominate, producing in excess of 90% of the signal events. General statements beyond this concerning the H^0 and A^0 admixture present in the signal seem elusive. Throughout the $\widetilde{\chi}_2^0\widetilde{\chi}_2^0$-dominated discovery region of Fig. 7, A^0 produced the majority of the events (though in some cases only slightly more than H^0); whereas in Fig. 8 there were substantial zones in which H^0 events dominated (as well as large segments wherein the two Higgs boson contributions were within $\sim$20% of each other). Finally, though the cuts did typically eliminate slightly more H^0 events than A^0 events, this effect was of little significance.

6.4 The topology of the signals

Note that in comparing the signal with the MSSM backgrounds, the present study follows the standard procedure of comparing signal and background rates at the same point in the MSSM parameter space. One could well ask whether or not larger backgrounds at a different point in parameter space could lead to the number of excess events attributed to the signal at the designated point in the MSSM parameter space. One way of addressing this issue is to look at the distribution of the signal+background events on a $M(e^+e^-)$ *vs.* $M(\mu^+\mu^-)$ wedgebox plot in addition to merely asking what is the raw rate. To wit, analyses of selected points in parameter space, again at the full event generator + detector simulation level, are presented illustrating that: (1) small changes in the MSSM input parameters can lead to significant topological changes in the pattern observed on the wedgebox plot; (2) the signal and background events often have markedly different distribution patterns on the wedgebox plot, pointing toward the possibility of further purifying cuts (perhaps in conjunction with extra information garnered from other studies or additional assumptions to clarify of what one is obtaining a purer sample) such as the example presented for plot (*a*) of Fig. 10; and (3) the composition of the $H^0, A^0 \to 4\ell + E_T^{\rm miss}$ signal, that is, what percentages are due to $H^0, A^0 \to \widetilde{\chi}_i^0\widetilde{\chi}_j^0$ for different i and j, may be ascertained to some level. The basic topological features of the wedgebox plot provide strong, often easily interpreted, leads as to which modes are the dominant contributors. The locations of the edges of such features on the wedgebox plot also provide information about the sparticle spectrum. The densities of event points in each component of wedgebox checkerboard can also be used to distinguish wedgebox plots with the same topological features/edges, such as, for instance, telling a wedgebox plot with a 2-3 wedge and a 2-2 box from one with only a 2-3 wedge. Further, these point density distributions may be used to reconstruct information about the relative production rates of the different $H^0, A^0 \to \widetilde{\chi}_i^0\widetilde{\chi}_j^0$ processes, though extracting such 'dynamical' information may well be far more complicated than is the task of extracting 'kinematical' information about the sparticle spectrum from the locations of the edges. All of this is further complicated by the remaining background events, and a more holistic study looking at both the Higgs boson produced signal and the MSSM backgrounds together may be most appropriate [48].

Note

Motivated in part by the earlier archival submission of this work, a similar analysis was eventually carried out by a member of ATLAS [54], also aiming at mapping out MSSM Higgs boson discovery regions via $H^0, A^0 \to \widetilde{\chi}_i^0 \widetilde{\chi}_j^0$ decays. Results of this ATLAS analysis are essentially consistent with those presented herein, though the actual shapes of the discovery regions obtained differ somewhat. These differences are in part attributable to adopting different selection criteria and employing different simulation tools. Of particular note are the $t\bar{t}$ and $b\bar{b}Z^{0(*)}$ backgrounds which are quite significant in the case of the ATLAS analysis but yield no background events in this study[38]. This is mainly due to the more stringent lepton isolation criteria adopted for this study which are very effective at removing leptons produced in these two would-be background processes from B-mesons decays. The restrictions on E_T^{ℓ}, which are absent from [54], also aid in removing residual background events.

Acknowledgments

The authors thank the organizers of the 2003 Les Houches workshop in association with which earlier stages of this work were performed. We also thank Guang Bian for assistance in preparing a couple of the figures. Communications with Simonetta Gentile are gratefully acknowledged. This work was supported in part by National Natural Science Foundation of China Grant No. 10875063 to MB and a Royal Society Conference Grant to SM, who is also supported in part by the program 'Visiting Professor - Azione D - Atto Integrativo tra la Regione Piemonte e gli Atenei Piemontesi'.

References

[1] J.F. Gunion, H.E. Haber, G.L. Kane and S. Dawson, "The Higgs Hunter Guide" (Addison-Wesley, Reading MA, 1990), *Erratum*, `hep-ph/9302272`.

[2] A. Djouadi, Phys. Rep. **459**, 1 (2008).

[3] S. Heinemeyer, W. Hollik and G. Weiglein, Phys. Rep. **425**, 265 (2006).

[4] S. Heinemeyer, `hep-ph/0807.2514`.

[5] S. Moretti, Pramana **60**, 369 (2003).

[6] K.A. Assamagan, A. Deandrea and P.-A. Delsart, Phys. Rev. D **67**, 035001 (2003).

[7] H. Baer, M. Bisset, D. Dicus, C. Kao and X. Tata, Phys. Rev. D **47**, 1062 (1993).

[8] H. Baer, M. Bisset, C. Kao and X. Tata Phys. Rev. D **50**, 316 (1994).

[9] F. Moortgat, S. Abdullin and D. Denegri, `hep-ph/0112046`.

[38] Simulations of 40 million $b\bar{b}Z^{0(*)}$ ($t\bar{t}$) events yielded 1(0) event(s) passing the set of selection cuts.

[10] C. Charlot, R. Salemo and Y. Sirois, J. Phys. G **34**, N1 (2007).

[11] P. Huang, N. Kersting and H.H. Yang, Phys. Rev. D **77**, 075011 (2008).

[12] M. Bisset, Univ. of Hawaii at Manoa Ph.D. Dissertation, UH-511-813-94 (1994).

[13] M. Bisset, M. Guchait and S. Moretti, Eur. Phys. J. C **19**, 143 (2001).

[14] CMS Collaboration Technical Design Report, Volumn II, J. Phys. G: Nucl. Part. Phys. **34**, 995 (2007). See page 380.

[15] M. Bisset and L. Ran, work in progress.

[16] ATLAS Collaboration, ATLAS detector and physics performance: Technical Design Report, Volume II, CERN-LHCC-99-015, May 1999, chapter 20, page 816. Using results from H. Baer, C.-H. Chen, F.E. Paige and X. Tata, Phys. Rev. D **52**, 2746 (1995).

[17] C. Caso *et al.*, Eur. Phys. J. C **3**, 1 (1998).

[18] A. Djouadi, M. Drees and J.L. Kneur, J. High Energy Phys. **0108**, 055 (2001), J. High Energy Phys. **0603**, 033 (2006).

[19] M. Battaglia *et al.*, Eur. Phys. J. C **22**, 535 (2001); F. Mahmoudi, J. High Energy Phys. **0710**, 026 (2007); O. Buchmueller *et al.*, J. High Energy Phys. **0809**, 117 (2008); J.R. Ellis J.S. Lee and A. Pilaftsis, J. High Energy Phys. **0810**, 049 (2008); C.F. Berger, J.S. Gainer, J.L. Hewett and T.G. Rizzo, `arXiv:0812.0980 [hep-ph]`.

[20] M. Bisset, F. Moortgat and S. Moretti, Eur. Phys. J. C **30**, 419 (2003).

[21] H. Baer and X. Tata, Phys. Rev. D **47**, 2739 (1993).

[22] P. Huang, N. Kersting and H.H. Yang, `arXiv:0802.0022 [hep-ph]`

[23] M. Bisset, R. Lu, N. Kersting, `arXiv:0806.2492 [hep-ph]`

[24] M. Bisset, N. Kersting, J. Li, S. Moretti and F. Moortgat, in `hep-ph/0406152`.

[25] K.A. Assamagan *et al.*, in `hep-ph/0002258`.

[26] K.A. Assamagan *et al.*, in `hep-ph/0203056`.

[27] M. Bisset, N. Kersting, J. Li, F. Moortgat, S. Moretti and Q. L. Xie, Eur. Phys. J. C **45**, 477 (2006).

[28] See: `http://www.cern.ch/LEPSUSY/`
and/or `http://lepsusy.web.cern.ch/lepsusy/` .

[29] See: `http://lephiggs.web.cern.ch/LEPHIGGS/papers/`.

[30] H. Baer, F.E. Paige, S.D. Protopopescu and X. Tata, `hep-ph/0001086`.

[31] T. Ibrahim, Phys. Rev. D **77**, 065028 (2008).

[32] F. Maltoni, Z. Sullivan and S.S.D. Willenbrock, Phys. Rev. D **67**, 093005 (2003); F. Maltoni, T. McElmurry and S.S.D. Willenbrock, Phys. Rev. D **72**, 074024 (2005).

[33] V. Del Duca, W. Kilgore, C. Oleari, C. Schmidt and D. Zeppenfeld, Nucl. Phys. B **616**, 367 (2001).

[34] J. Pumplin *et al.* (CTEQ Collaboration), J. High Energy Phys. **0207**, 012 (2002), D. Stump *et al.* (CTEQ Collaboration), J. High Energy Phys. **0310**, 046 (2003).

[35] S. Moretti, K. Odagiri, P. Richardson, M.H. Seymour and B.R. Webber, J. High Energy Phys. **0204**, 028 (2002).

[36] G. Corcella *et al.*, J. High Energy Phys. **0101**, 010 (2001).

[37] G. Corcella *et al.*, `hep-ph/0210213`.

[38] G. Corcella *et al.*, `hep-ph/9912396`, `hep-ph/0107071`, `hep-ph/0201201`; see also: `http://www-thphys.physics.ox.ac.uk/users/PeterRichardson/HERWIG/isawig.html`.

[39] M. Bisset, P. Roy and S. Raychaudhuri, `hep-ph/9602430`.

[40] H. Baer, C.-H. Chen, F. Paige and X. Tata, Phys. Rev. D **49**, 3283 (1994).

[41] A. Djouadi, J. Kalinowski and M. Spira, Comput. Phys. Commun. **108**, 56 (1998).

[42] S. Moretti, L. Lonnblad and T. Sjostrand, J. High Energy Phys. **9808**, 001 (1998).

[43] H. Baer, M. Bisset, C. Kao and X. Tata, Phys. Rev. D **46**, 1067 (1992).

[44] T. Sjostrand, `hep-ph/9508391`.

[45] See Fig. 19-82 on page 774 of [16]. Also Fig. 3.14 in T. Abe *et al.*, `hep-ex/0106056`.

[46] S. Gennai *et al.*, Eur. Phys. J. C **52**, 383 (2007).

[47] S. Zmushko *et al.*, ATL-COM-PHYS-1999-005, ATL-COM-PHYS-1998-009.

[48] G. Bian, M. Bisset, N. Kersting, Y. Liu, and X. Wang, Eur. Phys. J. C **53**, 429 (2008).

[49] G. Bian, M. Bisset, N. Kersting and R. Lu, work in progress.

[50] F.E. Paige, `hep-ph/9609373`.

[51] K. Kawagoe, M.M. Nojiri and G. Polesello, Phys. Rev. D **71** (2005) 035008; M.M. Nojiri, G. Polesello and D.R. Tovey, `hep-ph/0312317`; M.M. Nojiri, `hep-ph/0411127`.

[52] C. Hansen, N. Gollub, K. Assamagan and T. Ekelof, Eur. Phys. J. C **44S2**, 1 (2005) [*Erratum-ibid.* C **44S2**, 11 (2005)].

[53] S. Moretti, in preparation.

[54] S. Gentile [ATLAS Collaboration], ATL-COM-PHYS2008-225, ATL-PHYS-PROC-2008-077 and ATL-PHYS-PROC-2009-020.